Energy Conversion and Management 169 (2018) 45–77

Contents lists available at ScienceDirect

Energy Conversion and Management

journal homepage: www.elsevier.com/locate/enconman

Characterization of aerodynamic performance of vertical axis wind turbines: Impact of operational parameters

Abdolrahim Rezaeiha[a,*], Hamid Montazeri[a,b], Bert Blocken[a,b]

[a] Building Physics and Services, Department of the Built Environment, Eindhoven University of Technology, P.O. Box 513, 5600 MB Eindhoven, The Netherlands
[b] Building Physics Section, Department of Civil Engineering, KU Leuven, Kasteelpark Arenberg 40 – Bus 2447, 3001 Leuven, Belgium

ARTICLE INFO

Keywords:
Darrieus H-type VAWT
Tip speed ratio
Reynolds number
Turbulence intensity
Dynamic loads
Turbine wake

ABSTRACT

Vertical axis wind turbines (VAWTs) have received growing interest for off-shore application and in the urban environments mainly due to their omni-directional capability, scalability, robustness, low noise and costs. However, their aerodynamic performance is still not comparable with their horizontal axis counterparts. To enhance their performance, the impact of operational parameters such as tip speed ratio (λ), Reynolds number (Re_c) and turbulence intensity (TI) on their power performance and aerodynamics needs to be deeply understood. The current study, therefore, intends to systematically investigate the effect of these parameters in order to provide a deeper insight into their impact on the aerodynamic performance of VAWTs. For this investigation, a Darrieus H-type VAWT has been employed. A wide range of the parameters is considered: $\lambda = 1.2–6.0$, $Re_c = 0.3 \times 10^5–4.2 \times 10^5$ and $TI = 0\%–30\%$ to analyze the turbine performance, turbine wake and dynamic loads on blades. High-fidelity computational fluid dynamics (CFD), extensively validated with experimental data, are employed. The results show that (i) variable-speed operation maintaining the optimal λ at different wind speeds improves the turbine power coefficient, e.g. up to 168% at 4 m/s, while keeping an almost constant thrust coefficient, (ii) the turbine performance and wake are Re-dependent up to the highest Re_c studied, (iii) large TI (> 5%) improves the turbine performance in dynamic stall by promoting the laminar-to-turbulent transition and delaying stall on blades, however it deteriorates the optimal performance by introducing extra skin friction drag. The findings of the current study can support more accurate performance prediction of VAWTs for various operating conditions and can help the improvement of the aerodynamic performance of VAWTs.

1. Introduction

Vertical axis wind turbines (VAWTs) have received growing interest [1–7] for off-shore applications [8–10] as well as the built environment where they have the potential to be installed on the roof [11], included in the façade [12–15] or between buildings [16]. The installation can also be integrated in the ventilation ducts [17,18] and wind catchers [19–22]. The growing interest in the use of VAWTs could be attributed to several advantages such as [19,23–28]:

- Omni-directional capability: no yaw system is needed.
- Very low noise: due to operating at relatively low tip speed ratios and small diameters, the blade tip speed is very low.
- Low manufacturing cost: due to simple blade profiles with no taper and twist as well as simplicity in the control system, i.e. no pitch and yaw control system.
- Low installation and maintenance costs: due to having the generator on the ground.
- Scalability: the turbine height can scale up with minimal effect on performance.
- Robustness and reliability.
- Very small shadow flickering.
- Birds safety: due to their shape and typically low installation height
- Visually attractive.
- Multifaceted installation tower, e.g. telecom towers
- High space efficiency: VAWTs have smaller plan area compared to HAWT of the same swept area.

However, the aerodynamic performance of VAWTs is currently lower than HAWTs [29–32]. Research on VAWTs, despite their complex aerodynamics, has been situated in the shadow of the studies on HAWTs and hence received comparatively little attention during the last decades [33]. The underlying physics behind the power generation of VAWTs is much more complex compared to HAWTs [34–40]. The complexity could be mainly attributed to the VAWT's inherent unsteady power conversion due to the large variations of angle of attack and the

* Corresponding author.
E-mail address: a.rezaeiha@tue.nl (A. Rezaeiha).

https://doi.org/10.1016/j.enconman.2018.05.042
Received 24 February 2018; Received in revised form 11 May 2018; Accepted 12 May 2018
Available online 26 May 2018

Nomenclature

A	turbine swept area, $h{\cdot}d$ [m^2]
c	blade chord length [m]
C_d	sectional drag coefficient, $D/(0.5\rho c V_{rel}^2)$ [–]
C_{Fn}	instantaneous normal force coefficient [–]
C_{Ft}	instantaneous tangential force coefficient [–]
C_l	sectional lift coefficient, [–]
C_m	instantaneous moment coefficient [–]
C_P	power coefficient, $P/(qAU_\infty)$ [–]
C_T	thrust coefficient, $T/(qA)$ [–]
CoP	pressure coefficient [–]
D	sectional drag force [N/m]
d	turbine diameter [m]
h	turbine height [m]
k	turbulence kinetic energy [m^2/s^2]
K	reduced frequency, $\Omega c/(2V_{rel})$ [–]
L	sectional lift force [N/m]
L_w	turbine wake length [m]
M	turbine moment [Nm]
n	Number of blades [–]
P	turbine power [W]
q	dynamic pressure [Pa]
R	turbine radius [m]
Re_c	airfoil (blade) chord-based Reynolds number [–]
Re_θ	Momentum-thickness Reynolds number [–]
T	turbine thrust force [N]
TI	approach-flow total turbulence intensity [%]
TI_i	incident-flow total turbulence intensity [%]
$\overline{u}$	time-averaged streamwise velocity [m/s]
V	velocity magnitude [m/s]
V_n	normal velocity [m/s]
V_t	tangential velocity [m/s]
U_i	induced velocity [m/s]
U_∞	freestream velocity [m/s]
$\overline{v}$	time-averaged lateral velocity [m/s]
V_{rel}	relative velocity [m/s]
$V_{rel,geo}$	geometrical relative velocity [m/s]
W	domain width [m]
X/c	dimensionless chordwise position along the blade [–]
α	angle of attack [°]
α_{geo}	geometrical angle of attack [°]
α_i	induced angle of attack due to induced velocity [°]
α_{ss}	static stall angle [°]
γ	intermittency [–]
θ	azimuth angle [°]
λ	tip speed ratio [–]
ν	kinematic viscosity of air [m^2/s]
σ	solidity [–]
ω	specific dissipation rate [1/s]
Γ	circulation [m^2/s]
Ω	turbine rotational speed [rad/s]
Ω_{opt}	optimal turbine rotational speed [rad/s]
LSB	laminar separation bubble

relative velocity during each turbine revolution [23]. In addition, this can be accompanied by several complex flow phenomena such as dynamic stall [41,42], blade-wake interaction [43], flow curvature effects [44], Coriolis and centrifugal forces on the boundary layer of the rotating blades and the shed vortices [45]. In order to improve the aerodynamic performance of VAWTs, therefore, these flow complexities need to be well understood. In addition, the impact of various geometrical parameters and operational parameters on the aerodynamic performance of VAWTs needs to be comprehensively characterized. The geometrical parameters include number of blades [46–48], solidity [49–51], airfoil shape [52–54], blade pitch angle [23] and turbine shaft [55]. The operational parameters consist of tip speed ratio [56–61], Reynolds number [61–65] and turbulence intensity [58,66–68]. The focus of the present study is on the impact of the aforementioned operational parameters.

Tip speed ratio λ is one of the most important operational

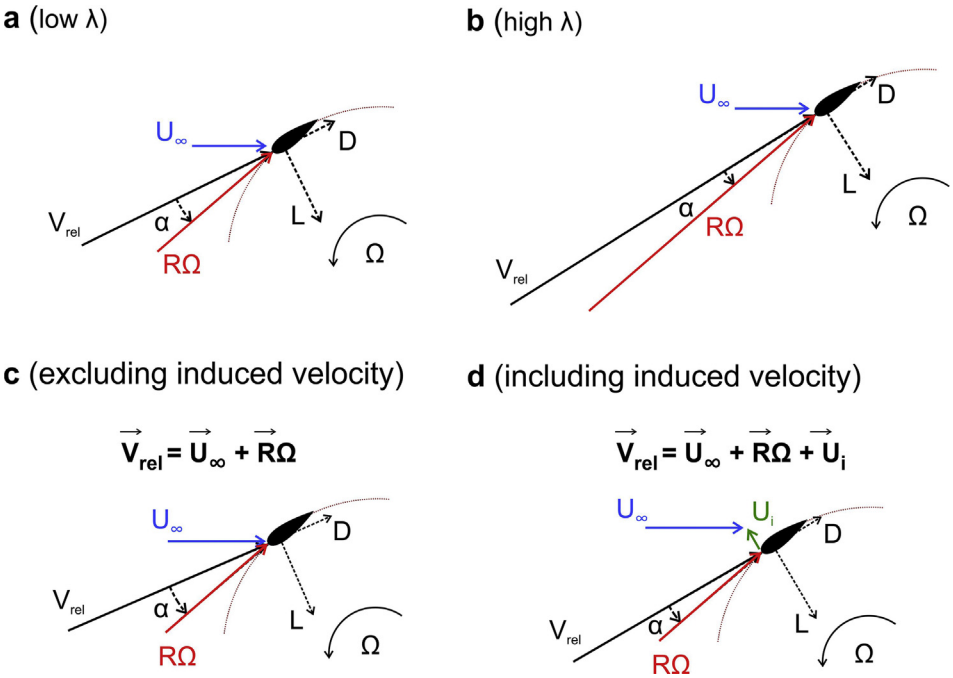

Fig. 1. Schematic of velocity triangle on a VAWT blade showing the difference between: (a and b) low versus high tip speed ratio, (c and d) considering versus ignoring the induced velocity (not to scale).

Table 1
Geometrical and operational characteristics of the reference turbine.

Parameter	Value
Number of blades, n	2
Diameter, d [m]	1
Swept area, A [m^2]	1
Airfoil	NACA0018
Airfoil chord, c [m]	0.06
Solidity, σ	0.12
Blade aspect ratio, h/c	16.67
Shaft diameter [m]	0.04
Tip speed ratio, λ	4.5
Rotational speed, Ω [rad/s]	83.8
Freestream velocity, U_∞ [m/s]	9.3
Chord-based Reynolds number, Re_c	1.76×10^5
Freestream (approach-flow) total TI [%]	5
Turbulence length scale [m]	1
Reduced frequency, K	0.06

parameters for VAWTs as it defines the range of variations of angle of attack (Δα) on blades during each turbine revolution. Low λ values correspond to large Δα (Fig. 1a) that could result in significant flow separation and the consequent power loss, if the stall angle is exceeded. On the other hand, high λ values correspond to small Δα (Fig. 1b), which could also mean that the blade is producing less power than its actual capability. Neither of the two cases are desired. Therefore, it is very important to deeply clarify the impact of λ on the aerodynamic performance of VAWTs. Note that the velocity triangle on a VAWT blade includes the induced velocity U_i. The induced velocity, which is usually ignored for simplicity, will affect the calculated α and relative velocity V_{rel} (see Fig. 1c and d) and consequently the loads on blades. The importance of considering the induced velocity in the aerodynamic performance calculations for VAWTs is further discussed in the Appendix A.

Numerous studies have been performed to provide insight on the impact of λ for VAWTs [56–61]. However, the vast majority of these studies focused on the impact of λ on power coefficient C_P, while less attention has been paid to the detailed analysis of aerodynamics and dynamic loads on turbine blades. In addition, these studies did not investigate the optimal turbine operation by maintaining the optimal λ versus wind speed. Such investigations could highlight the benefits of maintaining the optimal tip speed ratio for VAWTs.

The prime effect of Reynolds number (Re) on boundary layer events and the aerodynamic performance of static airfoils is well shown in the literature [69–75]. The performance of VAWTs highly depends on the flow development over the blades, which have airfoil cross section. However, the presence of the two sources of unsteadiness, α and V_{rel} imposes significant differences in the boundary layer events compared to the static airfoils [23]. Therefore, the impact of Re on the dynamic

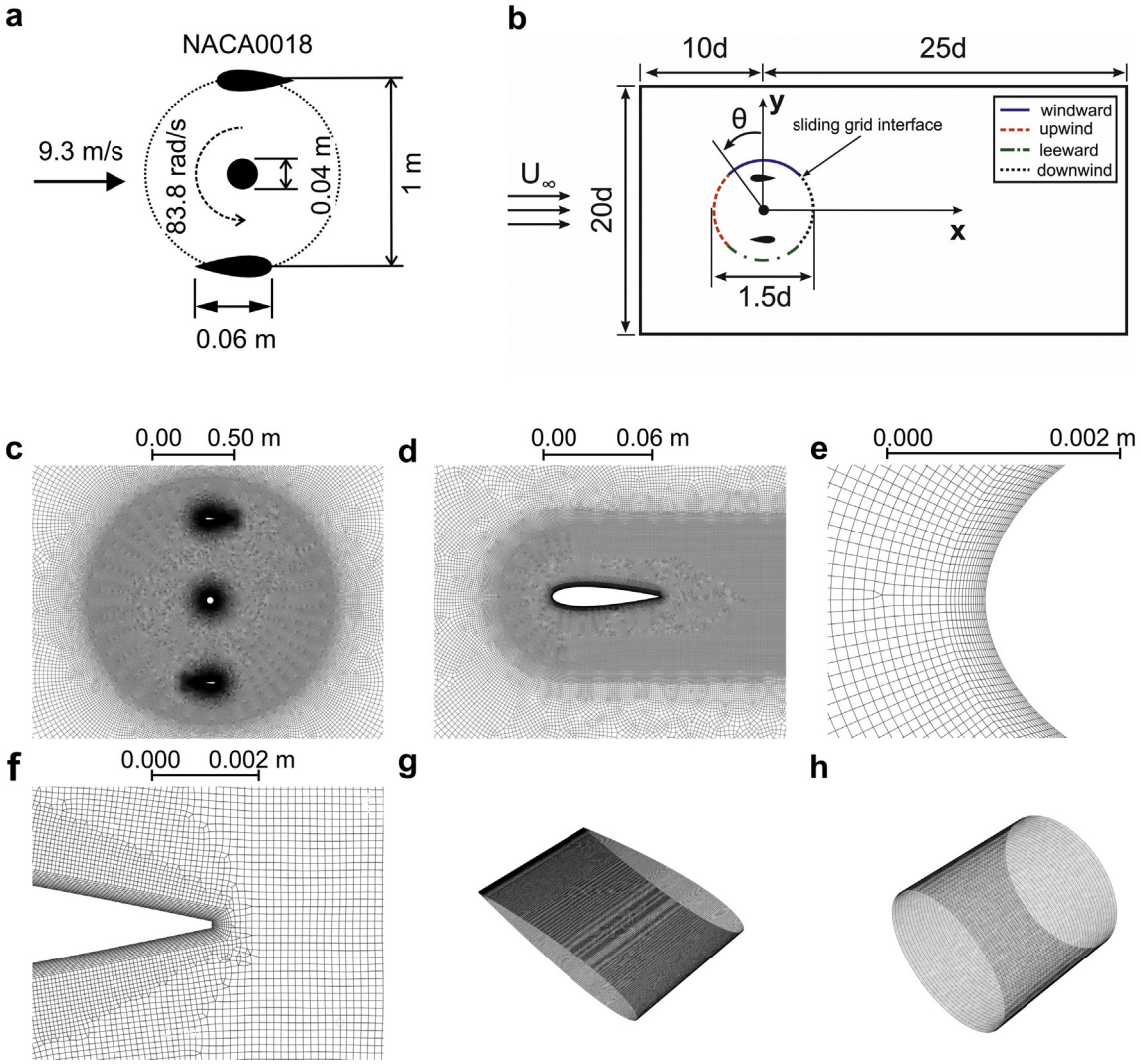

Fig. 2. Schematic of (a) the reference turbine and (b) the computational domain (both not to scale); (c–h) computational grid near the (c) rotating core, (d) airfoil, (e) leading edge, (f) trailing edge; and along the span for the (g) airfoil and (h) shaft.

loads on blades and the turbine performance cannot be simply adopted from the knowledge on static airfoils and demands a dedicated investigation.

For wind turbines, mainly due to size limitations, experiments are typically performed at small scales. This is especially the case when the wake effects and optimal arrangement of multiple turbines are investigated. This further emphasizes that the impact of Re on both turbine performance and wake needs to be well understood in order to enable a realistic interpretation of the scaled experiments for full-scale prototypes.

The high sensitivity of the VAWT performance to Re has been studied by Blackwell et al. [62], Polagye et al. [63], Bravo et al. [64], Bachant and Wosnik [65], Araya and Dabiri [61] and Zanforlin and Deluca [76]. While these studies have provided valuable findings, they did not focus on the impact of Re on blade aerodynamics and dynamic loads.

The importance of freestream turbulence on the separation behavior and the overall performance of airfoils [77] and HAWTs [78] is well established. It should be noted that while numerical and experimental studies of wind turbines are typically performed at a fixed turbulence level, in a real operating condition, such as in the urban environment, freestream turbulence intensity is varies widely [70,79–81]. Research on the impact of turbulence intensity for VAWTs is scarce and limited to few studies [58,66–68], which narrowed their scope on variations in C_P. To the best of our knowledge, however, a comprehensive study on the impact of TI on the aerodynamics, power performance and wake of VAWTs has not yet been performed.

Therefore, the current study intends to address these gaps by probing into the impact of λ, Re_c and TI on:

- Dynamic loads on blades: the variations of geometrical and experienced angle of attack, relative velocity, lift, drag and pressure coefficients and vorticity fields;
- Turbine performance: turbine power and thrust force, instantaneous tangential and normal loads on blades and the contribution of each turbine quartile in power production;
- Turbine wake: the instantaneous wake generation by a single blade and the mean velocity profiles in the wake.

The findings of this study are of paramount importance as they can significantly improve the accuracy of the performance predictions of VAWTs for different operating conditions. In addition, the results support the improvement of the design of VAWTs with respect to the target operating conditions.

The outline of the paper is: Section 2 describes the computational settings and parameters where the details of the studied turbine, the computational domain and grid and other numerical settings are presented. Section 3 briefly explains the verification and validation studies. The impact of tip speed ratio, Reynolds number and turbulence intensity are presented and discussed in Sections 4–6. The summary and conclusions are provided in Section 7.

2. Computational settings and parameters

A H-type vertical axis wind turbine with the geometrical and operational characteristics described in Table 1 is employed. The blade cross-section is the typical symmetrical NACA0018 airfoil. The geometrical and operational parameters of the reference turbine are selected with respect to the experimental study by Tescione et al. [82] employed for the validation (see Section 3). A schematic of the reference turbine is illustrated in Fig. 2a. The turbine and shaft rotate counter-clockwise with the same rotational velocity.

For the reference case, the approach-flow total TI is 5% (see Table 1), while the incident-flow total TI is 4.42%. It should be noted that for CFD simulations of VAWTs the incident-flow TI (the value at the location of the turbine), rather than the approach-flow TI (freestream), should be reported as it represents the level of turbulence that is actually experienced by the turbine blades. The decay of the turbulence in the computational domains has been already shown for the urban flows [83–86] and VAWTs [87]. The turbulence length scale at the inlet of CFD simulations describes the size of the large energy-containing eddies in a turbulent flow. For the flow around a wind turbine, the size of such eddies is found to be in the order of the turbine diameter [88]. Therefore, in the present study, the turbulence length scale is selected equal to the turbine diameter, i.e. 1 m.

A two-dimensional (2D) and a 2.5D computational domain, as shown in Fig. 2b, are employed. The three-dimensional (3D) simulation is not considered as the focus of the present study is on the flow in the mid-plane of a turbine with high blade aspect ratio (h/c > 10) where the flow is minimally influenced by the 3D tip effects on the blades

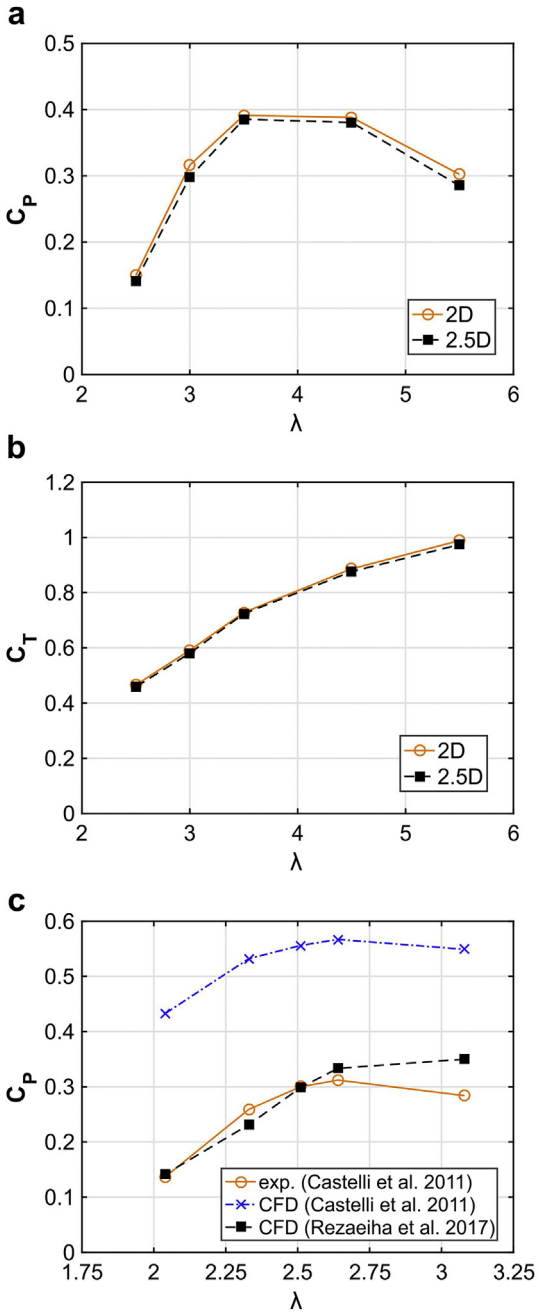

Fig. 3. Comparison of (a) power and (b) thrust coefficients for 2D and 2.5D simulations; (c) power coefficient against experimental and numerical results by Castelli et al. [104].

Table 2
Comparison of power coefficient from experiment by Castelli et al. [104] and the present CFD and their relative deviation.

λ	2.04	2.33	2.51	2.64	3.08
C_P (exp.)	0.137	0.259	0.300	0.312	0.284
C_P (present CFD)	0.142	0.231	0.299	0.333	0.350
$\|\Delta C_P\|$ [%]	3.42%	10.7%	0.5%	6.8%	23.2%

[82,89]. The h/c for the reference turbine is 16.67.

The 2D computational domain is 35d × 20d, where the distance from the turbine center to domain inlet and outlet are 10d and 25d, respectively. The blockage ratio (d/W) is 5%. The diameter of the rotating core is 1.5d. The computational domain is selected in line with the recently published guidelines for CFD simulations for VAWTs [87,90].

For 2.5D simulations, the sufficient spanwise domain size has been studied for the incompressible flows around airfoils and was found to be Re-dependent while for higher Re_c a smaller domain span would be required. For a NACA0012 airfoil at 10° angle of attack and $Re_c = 10^4$ a domain span of 0.64c was found to be sufficient [91] while for a NACA0015 airfoil at 16.6° angle of attack and $Re_c = 8.96 \times 10^5$, a domain span of 0.2c was proved to be adequate [92]. Therefore, for the present study on VAWTs, a larger spanwise domain length of 1c is selected as a safe choice. The 2.5D domain is only employed for the solution verification study for the 2D domain (see Section 3). The comparison of the 2D and 2.5D results for the reference turbine are provided in Section 3.

The turbine revolution is divided into 4 quartiles as listed below [93] where θ is defined based on the position of the top blade in Fig. 2.

- Upwind: $45° \le \theta < 135°$
- Windward: $315° \le \theta < 45°$
- Leeward: $135° \le \theta < 225°$
- Downwind: $225° \le \theta < 315°$

In addition, the turbine fore half, $0° \le \theta < 180°$, and the turbine aft half, $180° \le \theta < 360°$, are used to further assist with the interpretation of the results.

The computational grid, as shown in Fig. 2c–h, consists of quadrilateral cells with maximum and average y^+ values of 3.8 and 1.8, respectively, on the airfoil and 1.4 and 1.0, respectively, on the shaft. The number of cells are approximately 400,000 in 2D and 28 million in 2.5D. The 2D grid is extruded in spanwise direction to generate the 2.5D grid. The spanwise grid spacing is 0.5 mm and 1 mm for the airfoil and the shaft, respectively. Boundary conditions are uniform velocity inlet, zero gauge static pressure outlet, no-slip walls for airfoil and shaft, symmetry sides, sliding grid interface between the rotating and fixed grids, and periodic boundary condition on the top and bottom sides of the 2.5D domain.

Incompressible unsteady Reynolds-averaged Navier-Stokes (URANS) are performed using the commercial CFD software package ANSYS Fluent 16.1 with 2nd order discretization in time and space and SIMPLE scheme for pressure-velocity coupling. The numerical settings and simulation procedure are selected following extensive solution verification and validation studies performed by Rezaeiha et al. [23,55,87,90].

Given the transitional nature of the flow on a VAWT blade, considering Re_c, the transition SST turbulence model is used. This model is a 4-equation model [94] developed based on the 2-equation k-ω SST turbulence model [95,96], which additionally solves two more equations for momentum-thickness Reynolds number Re_θ and intermittency γ. The model, also known as γ-θ SST model, is an intermittency-based model. Intermittency-based models have been successfully used to improve the prediction of laminar-to-turbulent transition for flows on airfoils [97–101].

The simulations are initialized with steady RANS. The transient simulations are performed with azimuthal increment of 0.1° for 20 revolutions of the turbine. The 20 turbine revolutions are to ensure the results reach a statistically steady state condition. 20 iterations per time step is used to ensure scaled residuals drop below 10^{-5}. The results are sampled at the 21st turbine revolution.

To calculate the dynamic loads on blades, namely lift and drag, the experienced values of angle of attack and relative velocity, rather than the typically-used geometrical values, are employed. There exist noticeable differences between the geometrical and experienced values of the angle of attack, the relative velocity and their resultant loads on the blades. The calculation method for the experienced values and a comparison with the geometrical values are presented and discussed in the Appendix A.

3. Solution verification and validation

Extensive solution verification and two sets of validation have been performed to ensure the accuracy of the present CFD results. The results have been published in Ref. [87,90]. For solution verification studies:

- Grid dependence is analyzed using three uniformly doubled grids where the refinement factor in each directions is $\sqrt{2}$. The Grid Convergence Index (GCI) [102] for the coarse-medium grid pair, calculated for the turbine C_P using a safety factor (F_s) of 1.25, is $GCI^{coarse} = 0.0061$ (1.48% of the C_P value) and $GCI^{fine} = 0.0035$ (0.85% of the C_P value), respectively. The medium grid, also shown in Fig. 2c–f, is selected for the rest of the study.
- A detailed sensitivity analysis is performed for time step and convergence criterion [87,90]. The analysis shows that an azimuthal increment of 0.1° is the minimum requirement. In addition, a minimum of 20 turbine revolutions is required to reach a statistically steady state condition.
- The power and thrust coefficients for 2D and 2.5D simulations are compared [87] (shown in Fig. 3a and b). The comparison reveals a systematic but small overestimation of the turbine power performance for the 2D simulations. The 2D C_P and C_T values are ≤6% and ≤2% higher than that of the 2.5D simulations due to neglecting the three-dimensional effects in the boundary layer, which affect the transition and separation onsets on blades [103]. The analysis shows that the difference between the 2D and 2.5D simulations is weakly dependent on the operating conditions of the turbine. Note that that small difference between the 2D and 2.5D (< 6%) is in spite of the fact that the number of cells for the 2.5D simulations is approximately 28 million, which is 70 times more than that of the 2D grid, i.e. approximately 400,000 cells. Therefore, to minimize the computational cost, which is essential for extensive parametric studies such as the present study including 300 transient simulations each employing a fine azimuthal increment of 0.1° and continuing for minimum 20 turbine revolutions, the 2D simulations are selected to predict the turbine performance.

Two separate sets of validation studies have been performed where the CFD results have been compared against the experimental data by

Table 3
Operational parameters to study the impact of λ.

λ	2.5	3.0	3.5	4.0	4.5	5.5
U_∞ [m/s]	18.6	16.275	13.95	11.625	11.625	9.3
Ω [rad/s]	93	97.65	97.65	93	104.625	102.3
TI [%]	5	5	5	5	5	5
TI_i [%]	4.42	4.42	4.42	4.42	4.42	4.42
Re_c (× 10^5)	2.06	2.11	2.09	1.97	2.2	2.14
K	0.06	0.06	0.06	0.06	0.06	0.06

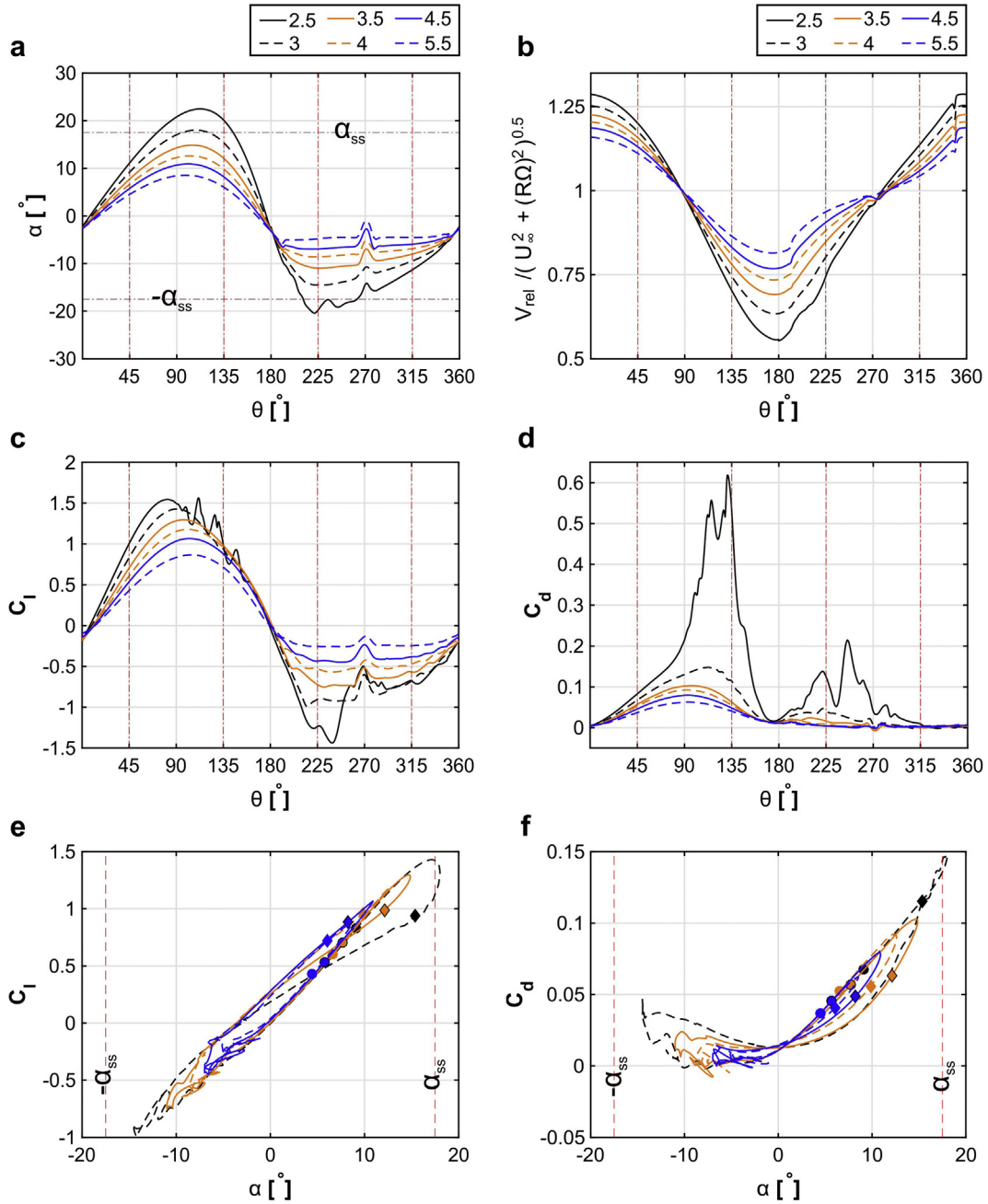

Fig. 4. Variations of (a) experienced angle of attack, (b) normalized relative velocity, (c) lift and (d) drag coefficients versus azimuth; (e) lift and (f) drag coefficients versus angle of attack; during the last turbine revolution for different tip speed ratios. α_{ss} denotes the inviscid static stall angle from Xfoil [106]. (○) and (◊) denote $\theta = 45^\circ$ and 135°, respectively. ($Re_c \approx 2.0 \times 10^5$).

Castelli et al. [104] and Tescione et al. [82]. Note that the turbines employed in the two experiments have different airfoil shape, number of blades, solidity and tip speed ratios. In addition, the parameters employed for the two validations are also different. The turbine for the first validation is a 2-bladed H-type turbine with NACA0018 airfoil, a solidity of 0.12 and a tip speed ratio of 4.5 (reference turbine). For this validation, the time-averaged normalized lateral and streamwise velocities at different downstream locations (x/R = 2.0–3.0) in the near wake of the turbine along the lateral direction are compared with the experimental results by Tescione et al. [82]. The deviation from the experiment is 2.3–2.5% and 8.6–11.8% for the lateral and streamwise velocity components, respectively. Further details and possible explanations for the observed deviation are comprehensively presented in Ref. [55,87]. The turbine for the second validation is a 3-bladed H-type turbine with NACA0021 airfoil, a solidity of 0.25 and tip speed ratios from 2.04 to 3.08. For this validation, the turbine power coefficients at 5 different tip speed ratios (i.e. 2.04, 2.33, 2.51, 2.64 and 3.08) are compared with experimental and numerical data by Castelli et al. [104] (see Fig. 3c). An overall good agreement is observed between the CFD results and the experiment where the quantitative differences, presented in Table 2, are found to be the largest for the highest λ of 3.08. The observed deviations could be explained to be a result of:

- The uncertainties associated with the experimental data: several important geometrical characteristics of the turbine, e.g. the blade surface roughness and the location of the blade-spoke connection, and the boundary conditions, e.g. the turbulence intensity and length scale, are not clearly mentioned in the experiment. For

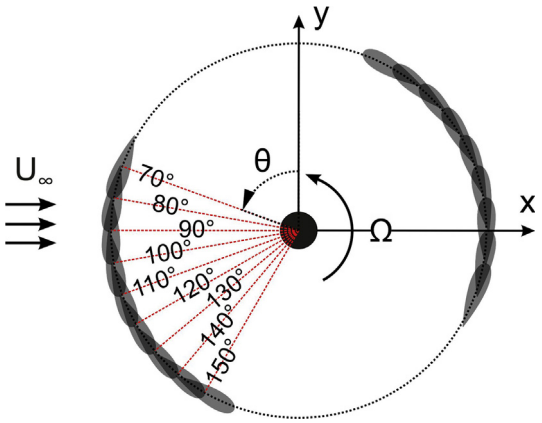

Fig. 5. The sampling locations discussed in Figs. 6, 7, 16 and 22.

instance, the impact of the location of the blade-spoke connection on the turbine C_P is known to be more pronounced at higher tip speed ratios [105]. This could somehow explain the larger deviation at higher λ.

- Lack of error analysis for the experiment: the experiment has not provided an error analysis of the data, therefore, the error associated with the measurement is not known. For instance, the blockage ratio for the experiment is considerable large (approximately 10%) while the measured values were not corrected for the blockage effects.
- Geometrical simplifications: ignoring the turbine spokes and connections in the CFD modeling is possibly contributing to the observed deviation. As these less-aerodynamic structural components typically result in considerable drag, their impact will be more pronounced at higher relative velocities, i.e. higher tip speed ratios. This could also justify the larger deviation at higher λ.
- The two-dimensional modeling: because the turbine is modeled in 2D, the blade tip effects are not considered in the simulations where ignoring them also partly contributes to the deviation.
- The RANS modeling: the limitations of RANS modeling in predicting complex flows around VAWTs could be another contributor to the observed deviation, esp. at lower λ where the flow becomes more complex due to dynamic stall.

Further information about this validation study with further explanations for the observed deviation is presented in detail in Refs. [23,90]. The two validation studies performed confirm that the CFD results can provide accurate predictions of the turbine performance and wake for different operating conditions.

4. Impact of tip speed ratio

This section provides an extensive analysis of the impact of λ on the dynamic loads on turbine blades, the turbine performance and the

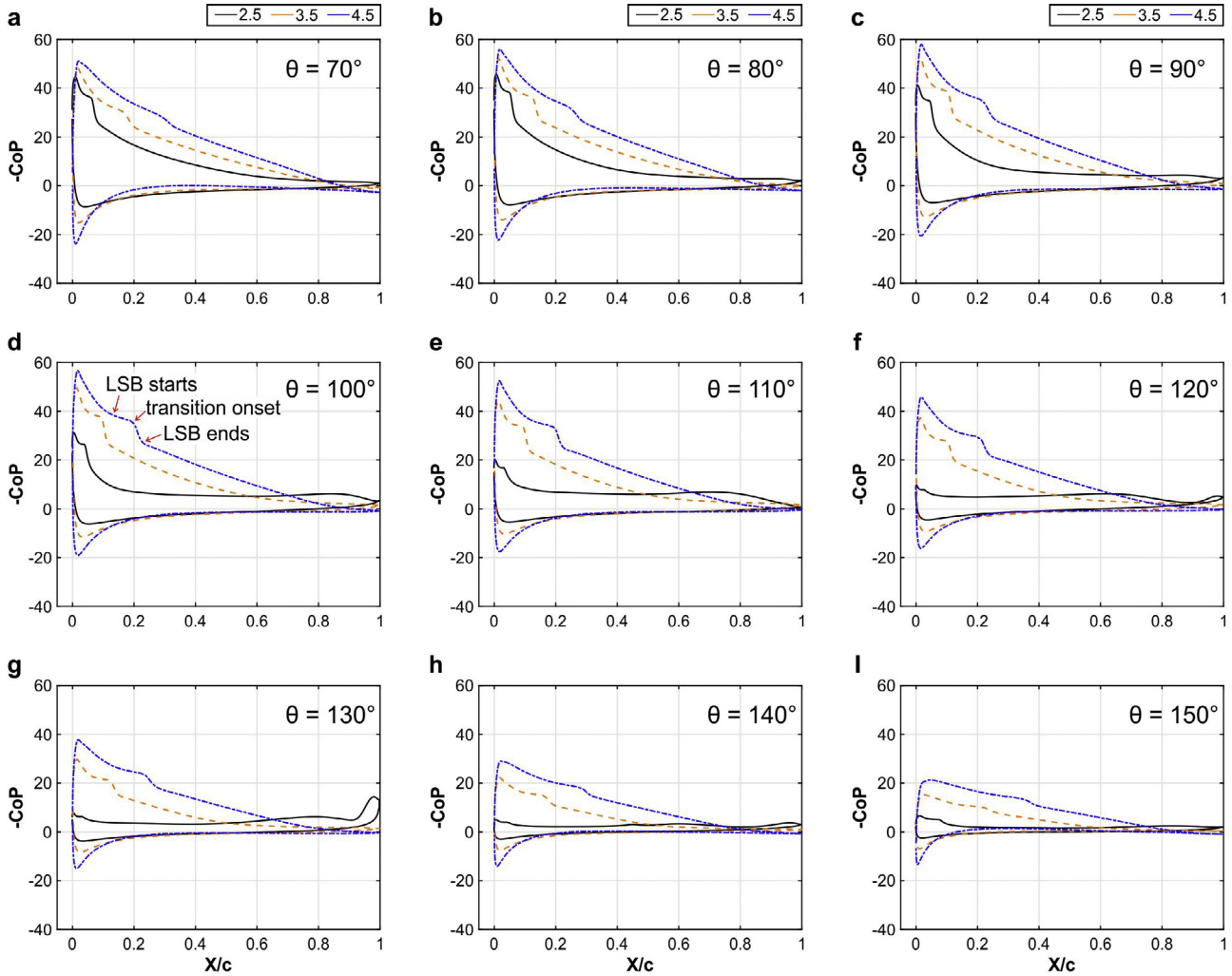

Fig. 6. Pressure coefficient (CoP) over the blade during the last turbine revolution for different tip speed ratios at azimuthal positions set in Fig. 5. X/c represents the dimensionless chordwise position along the blade. ($Re_c \approx 2.0 \times 10^5$).

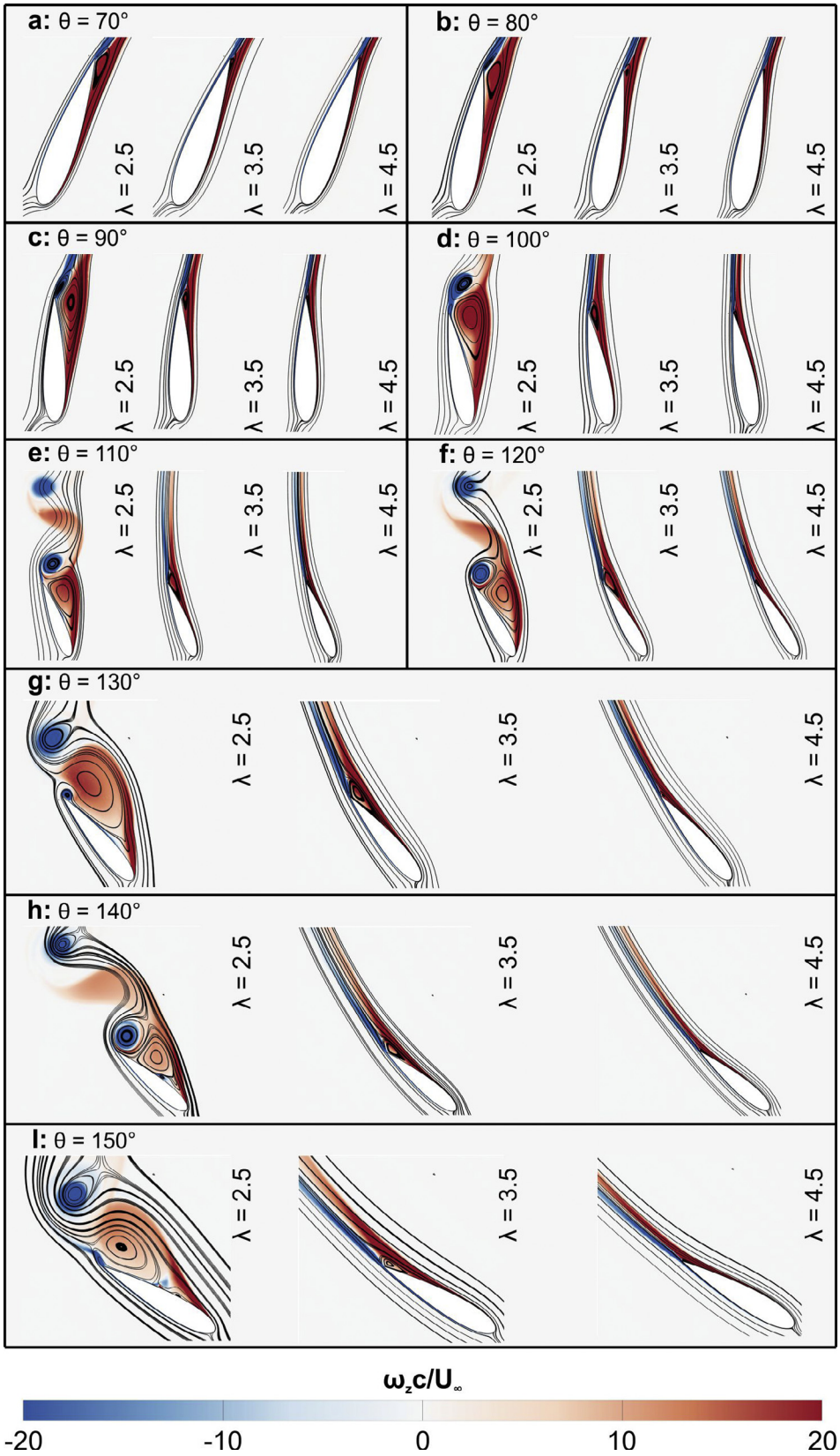

Fig. 7. Contours of non-dimensionalized z-vorticity with superimposed streamlines for different tip speed ratios during the last turbine revolution at azimuthal positions set in Fig. 5. ($Re_c \approx 2.0 \times 10^5$).

wake. Table 3 lists the operational parameters used to study the impact of λ. The tip speed ratios are selected to range from low, λ = 2.5, to moderately high, λ = 5.5, values for the given solidity of the reference turbine. The analysis is performed at a fixed Re_c of approximately 2.0×10^5, as a representative value for small- to medium-scale urban VAWTs [12]. The fixed Re_c avoids Reynolds number effects and facilitates a detailed analysis of the impact of tip speed ratio. To keep a fixed Re_c for different tip speed ratios, both freestream velocity and turbine rotational velocity are inevitably adjusted. The turbulence intensity and reduced frequency are kept the same as in the reference case. The approach-flow (incident-flow) total TI is 5% (4.42%) and the reduced frequency (defined as $K = \Omega c/(2V_{rel})$) is 0.06 for all cases.

4.1. Loads on blades

Fig. 4 shows the variations of α, normalized V_{rel}, lift and drag coefficients, C_l and C_d, during the last turbine revolution for $2.5 \leq \lambda \leq 5.5$. Two sources of flow unsteadiness on VAWT blades, namely unsteady α and V_{rel}, are shown in Fig. 4a and b where the values are calculated following the method described in the Appendix A. The following observations are made for the angle of attack α:

- In the turbine fore half, almost a half-cycle sinusoidal variation is observed for all cases.
- In the turbine aft half, the trend deviates from a sinusoidal trend and becomes nearly flat with increasing λ. The different trend in the turbine aft half is because the flow in this region is significantly affected by the blades passing in the turbine fore half and slowed down due to the turbine thrust force. The increase in flatness can also be explained by the increase in the thrust force for higher λ (see Section 4.2).
- A negative non-zero value of α occurs at θ = 0° and 180° due to the lateral deviation of the incoming flow at the turbine incidence (streamtube expansion).
- Decreasing λ, as expected, is found to increase the amplitude of variations of α throughout the revolution. This is simply explained by comparing the velocity triangles shown in Fig. 1a and b. For λ > 3.0, the variation of α remains below the static stall angle $\alpha_{ss} = 17.5°$, which is calculated from Xfoil [106] at $Re_c = 2.0 \times 10^5$. Further reduction in λ results in α reaching and exceeding α_{ss} both in fore and aft halves. A deep stall happens for λ = 2.5 in both halves.
- For λ = 2.5, the ripples observed at θ ≈ 225° are due to blade-wake interactions which will be later discussed in this section.
- The ratio of the magnitude of the negative peak, in the turbine aft half, to that of the positive peak, in the turbine fore half, decreases from 90% for λ = 2.5 to 54% for λ = 5.5.
- In the turbine aft half, the effect of the turbine shaft wake on α is also apparent as a sudden reduction near θ = 270°. The impact of the VAWT turbine shaft is extensively discussed in Ref. [55].

Fig. 4b depicts the other source of flow unsteadiness for VAWT, i.e. unsteady inflow to the blades. In the turbine fore half, the normalized V_{rel} oscillates sinusoidally where the amplitude of the oscillations increases from 17.5% at λ = 5.5 to 36.7% at λ = 2.5. In the turbine aft half, similar to α, a different trend is observed.

The two co-occurring sources of unsteadiness for VAWTs, namely unsteady α and V_{rel}, are known to have a different impact on boundary layer events, namely laminar-to-turbulent transition and separation, on airfoils [103], which further highlights the complexity of the dynamic loads on VAWTs. Fig. 4c and d show the dynamic lift and drag coefficients (C_l and C_d) versus azimuth θ for the last turbine revolution. The impact of λ on C_l is similar to that of λ on α although the peak for C_l occurs earlier for C_l. For λ = 2.5, the fluctuations in C_l and the large

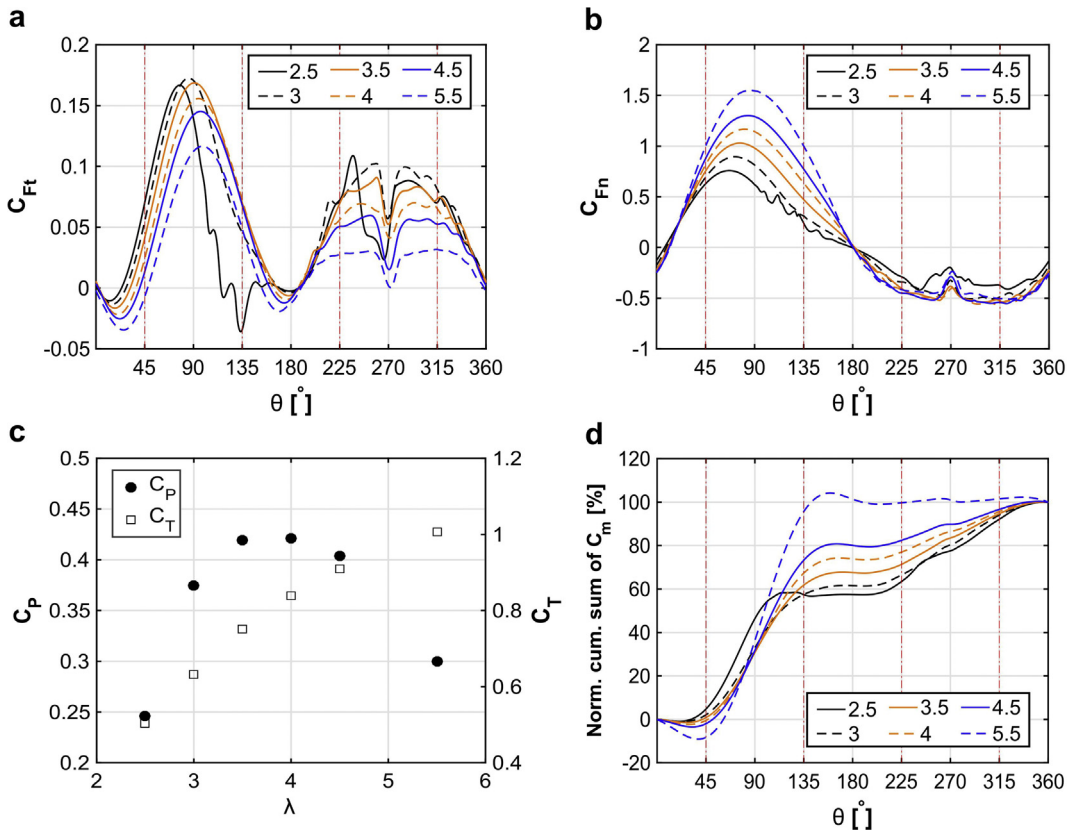

Fig. 8. Coefficients of (a) tangential force, (b) normal force, (c) power and thrust and (d) the normalized cumulative sum of moment coefficient during the last turbine revolution for different tip speed ratios. ($Re_c \approx 2.0 \times 10^5$).

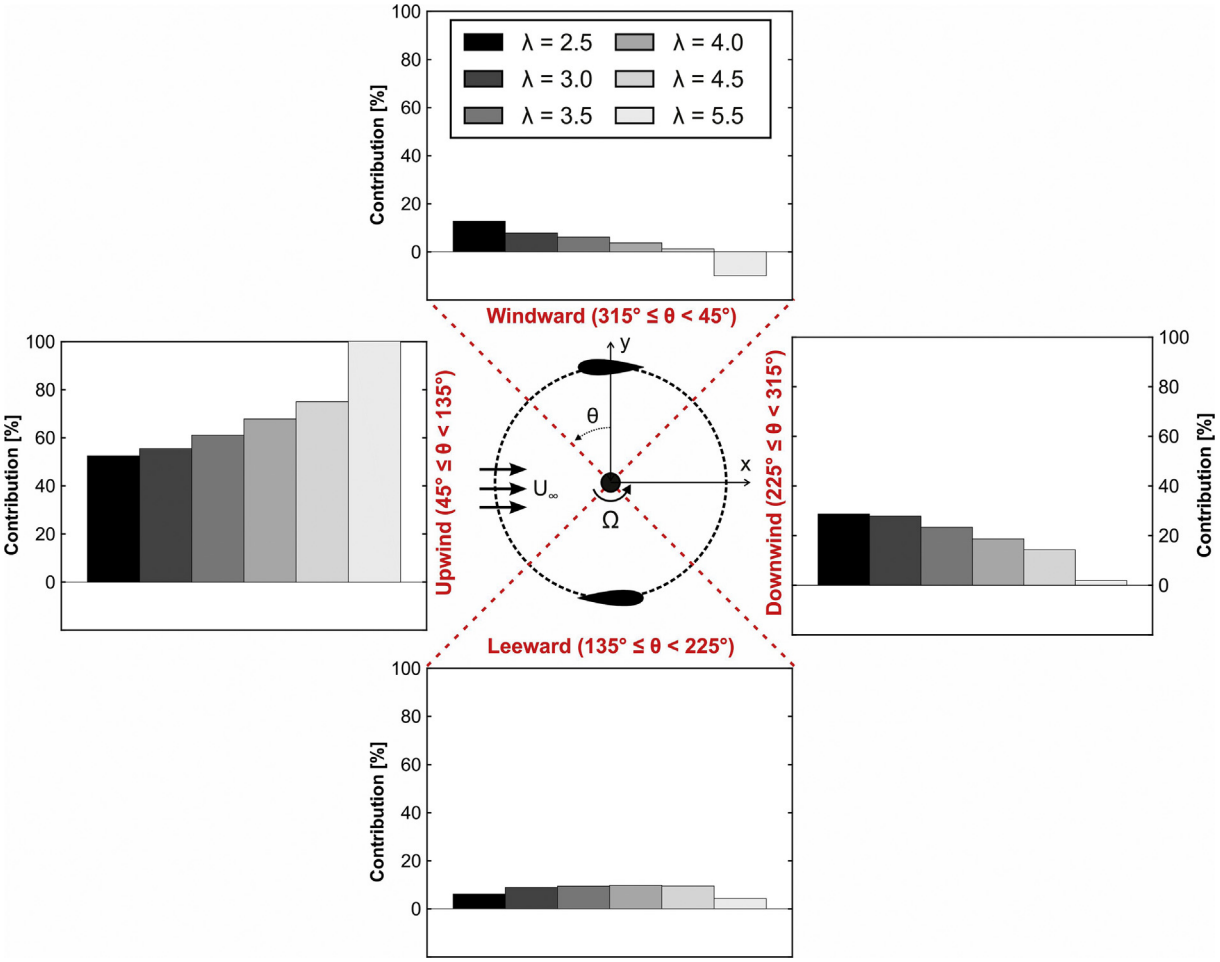

Fig. 9. Contribution of each revolution quartile to total turbine power for different λ.

jump in C_d at $90^\circ \leq \theta \leq 170^\circ$ clearly signal the stall on blades. The blade-wake interactions can be distinguished as large fluctuations in C_l and C_d at $220^\circ \leq \theta \leq 260^\circ$. The effect of the shaft wake is also observed around $\theta \approx 270^\circ$.

Fig. 4e and f show the dynamic C_l and C_d versus α for the last turbine revolution. Note that for better visualization of the impact of λ, the case of λ = 2.5 is not shown in these figures. The following observations can be made:

- The upwind quartile is shown using full circles (○) and diamonds (◊) signaling θ = 45° and 135°, respectively. It is clearly seen that this quartile is where the blades operate near $C_{l,max}$, $C_{d,max}$. The importance of this quartile will be more elaborately discussed in Section 4.2.
- Decreasing λ increases $C_{l,max}$, $C_{d,max}$ and the respective α for each.
- Decreasing λ marginally influences the hysteresis in the polars of both C_l and C_d prior to stall while near the stall, i.e. λ = 3.0, the hysteresis significantly increases. The hysteresis prior to stall is due to the presence of the unsteady separation on blades and the different resistance of the boundary layer to separation in the upstroke and downstroke [103]. The observations are in line with the experimental observations on pitching airfoils by Lee and Gerontakos [107].

To further analyze the impact of λ, the pressure coefficient on the blade and the flowfield at different azimuthal positions are compared for three different λ: 2.5, 3.5 and 4.5. The schematic shown in Fig. 5 illustrates the selected azimuthal positions. The respective positions along the α, C_l and C_d curves for the three λ can be found in Fig. 4a, c and d. The focus is on $70^\circ \leq \theta \leq 150^\circ$, which corresponds to the regime where the blade experiences the maximum α during the upstroke and downstroke.

Pressure coefficients (*CoP*) on the blade and contours of non-dimensionalized vorticity with superimposed streamlines are compared for different tip speed ratios in Figs. 6 and 7, respectively. It should be noted that the pressure distribution on the blade suction side (in the turbine fore half corresponding to the inner side of the blade) can be employed to identify the boundry layer events: (i) the sudden change in the rate of pressure recovery typically signals the beginning of a laminar separation bubble (LSB), (ii) the follow-up abrupt increase in pressure prompts laminar-to-turbulent transition onset (triggered by the Kelvin-Helmholtz instabilities in the shear layer of LSB) and (iii) the second sudden change in rate of pressure recovery shows the end of LSB, from which the length of LSB can also be estimated [108,109]. For further clarification, the aforementioned boundary layer events are highlighted with arrows for λ = 4.5 at θ = 100° (see Fig. 6d). The results show that:

- Laminar-to-turbulent transition onset occurs earlier for lower λ due to their higher α. This is in agreement with the experimental data for pitching airfoils where the transition onset is found to move towards the leading edge when α increases [107]. Previous CFD simulations ofVAWTs also confirmed similar occurrence, e.g. [23].
- The length of laminar separation bubble is shorter for lower λ due to higher α.
- For λ = 2.5, the increase of flatness in the *CoP* curve, which extends from $X/c \geq 0.6$ at θ = 70° to $X/c \geq 0.1$ at θ = 120°, implies the growth of the turbulent trailing edge separation over the blade. The

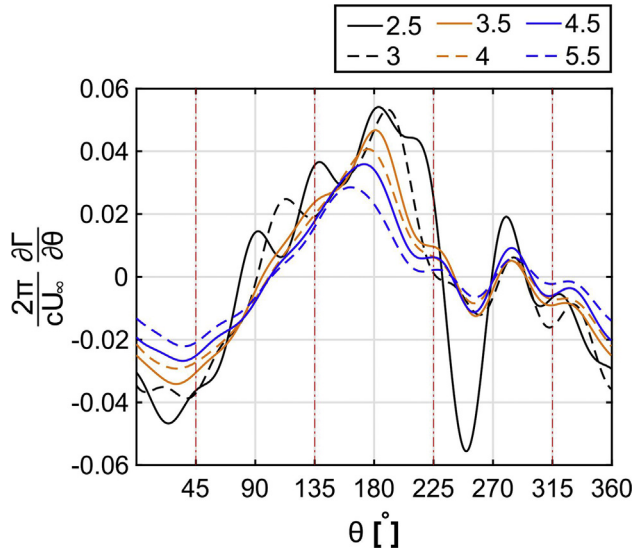

Fig. 10. Shed vorticity by a single blade during the last revolution for different tip speed ratios. Positive values denote counter-clockwise circulation based on the Kutta–Joukowski theorem [111]. ($Re_c \approx 2.0 \times 10^5$).

growth of the trailing edge separation from θ = 70° to 120° can also be distinguished from the vorticity field (Fig. 7). For λ = 3.5 and 4.5, the extent of trailing edge separation is limited to X/c ≥ 0.6 and ≥ 0.8, respectively. The smaller separation for higher λ is due to their lower α.

- For λ = 2.5, from θ = 120° to 140°, a small bump is found to grow near the trailing edge on the *CoP* curve. This could be due to the clockwise vortices rolled up from the pressure side towards the suction side.
- For λ = 2.5, from θ = 100° to 150°, vortex shedding occurs from the blade. This results in oscillations in loads as already shown in Fig. 4c and d for C_l and C_d. The interaction of such shed vortices with the boundary layer on the blades passing downstream (220° ≤ θ ≤ 260°) causes oscillations in loads as already shown in Fig. 4c and d for C_l and C_d. The downwind region influenced by the blade-wake interactions is not straightly downstream of the stalled region but is slightly drifted towards the center of rotation. This is attributed to the impact of the Coriolis force on the shed vortices, which is consistent with the finding of Tsai and Colonis [45].

4.2. Turbine performance

The instantaneous tangential C_{Ft} and normal C_{Fn} force coefficients on the blades and the power C_P and thrust coefficients C_T during the last turbine revolution for different tip speed ratios are shown in Fig. 8a–c. It can be seen that:

- Changing λ results in a rather complex change in tangential loads for both fore and aft turbine halves. In contrast, higher λ simply results in higher positive normal loads in the turbine fore half. In the turbine aft half, the effect of λ on normal loads is much less noticeable except for λ = 2.5 where the flow is dominated by the occurrence of dynamic stall and blade-wake interactions.
- At the beginning of the revolution (0° ≤ θ ≤ 75°), decreasing λ results in higher tangential loads. This is a result of higher α and C_l for lower λ as shown in Fig. 4a and b.
- For 75° < θ ≤ 170°, the occurrence of a deep stall is observed for λ = 2.5 where C_{Ft} suddenly drops. This associates with the sudden drop in C_l and the jump in C_d as shown in Fig. 4c and d. The occurrence of stall is clearly seen as fluctuations in C_{Ft} and C_{Fn}. A negligible difference is observed in the tangential loads for 3 < λ < 5.5.
- In the turbine aft half, and for 220° ≤ θ ≤ 260°, the blade-wake interactions can be distinguished as fluctuations in C_{Ft} and C_{Fn}, especially for λ = 2.5.
- The effect of the shaft is seen as a drop in C_{Ft} and a jump in C_{Fn} in θ ≈ 270°.
- An optimum λ of 4.0 is found to maximize C_P.
- C_T grows with increasing λ. The trend is linear up to λ = 3.5 while it becomes asymptotic for λ > 3.5. This is in line with the experimental observations by Bachant and Wosnik [110].

The normalized cumulative sum of the instantaneous moment coefficients C_m during the last turbine revolution is shown in Fig. 8d. The values are employed to calculate the contribution of each turbine quartile in total power production, which is shown in Fig. 9. The contribution is calculated as the difference between the normalized cumulative sum of C_m at the end of each quartile and that at the beginning of that quartile. For a given λ, for example, if the cumulative sum at the beginning of a quartile has a negative value, due to prior negative moment, while high positive value exists at the end of the quartile, the difference (the contribution of that quartile) can be close to 100% or even more. In addition, if one quartile has a negative total contribution, the sum of contribution of the other three quartiles needs to be more than 100% so that the total contribution of all 4 quartiles is 100%.

- In the windward quartile, the contribution is very small and decreases from 12.7% to −9.9% when λ increases from 2.5 to 5.5. A negative contribution is observed for λ = 5.5 which simply means that the flow is tending to rotate the turbine in the opposite direction.
- In the upwind quartile, for all cases, more than 50% of the total power is produced. The contribution increases from 52.5% to 103.7% for λ from 2.5 to 5.5. The contribution higher than 100% for λ = 5.5 is due to the negative contribution of the windward quartile for this λ. For the optimal λ (= 4.0), the contribution of the upwind quartile is ≈ 68%.
- In the leeward quartile, the contribution is less than 10% for all cases. The highest contribution is 9.8% at the optimal λ.
- In the downwind quartile, the contribution decreases from 28.7% to 1.9% for λ from 2.5 to 5.5. The trend is reverse of that in the upwind. This is because the flow reaching the downwind quartile is not fresh as it already passed the blades in the upwind region. Therefore, if higher energy is extracted from the flow upstream, less is remained to be extracted downstream.

The analysis reveals a very important fact regarding the power production of VAWTs. The upwind quartile is contributing the most to the total power production and is by far the most important region for the turbine operation. As highlighted in Section 4.1 and 4.2, the operation of VAWTs is highly variable during the revolution due to the unsteady α and V_{rel} and this inherent unsteadiness occurs for all λ. From a practical point of view, given the unsteady aerodynamics, it is extremely difficult to improve the performance during the whole revolution. This analysis shows the local power enhancement strategies functioning in the upwind quartile can grant the maximum benefit, compared to the other quartiles, because any small improvement in this region can have large influences on the total power production due to the significant contribution of this quartile.

4.3. Turbine wake

The turbine wake is generated from the vortices shed from the blades during the revolution. Based on Kelvin's circulation theorem [111], when the strength of the bound vortices along the blade alters, a new vortex is shed, with the same strength but the opposite sign, which travels downstream with the incoming flow. The change in the bound

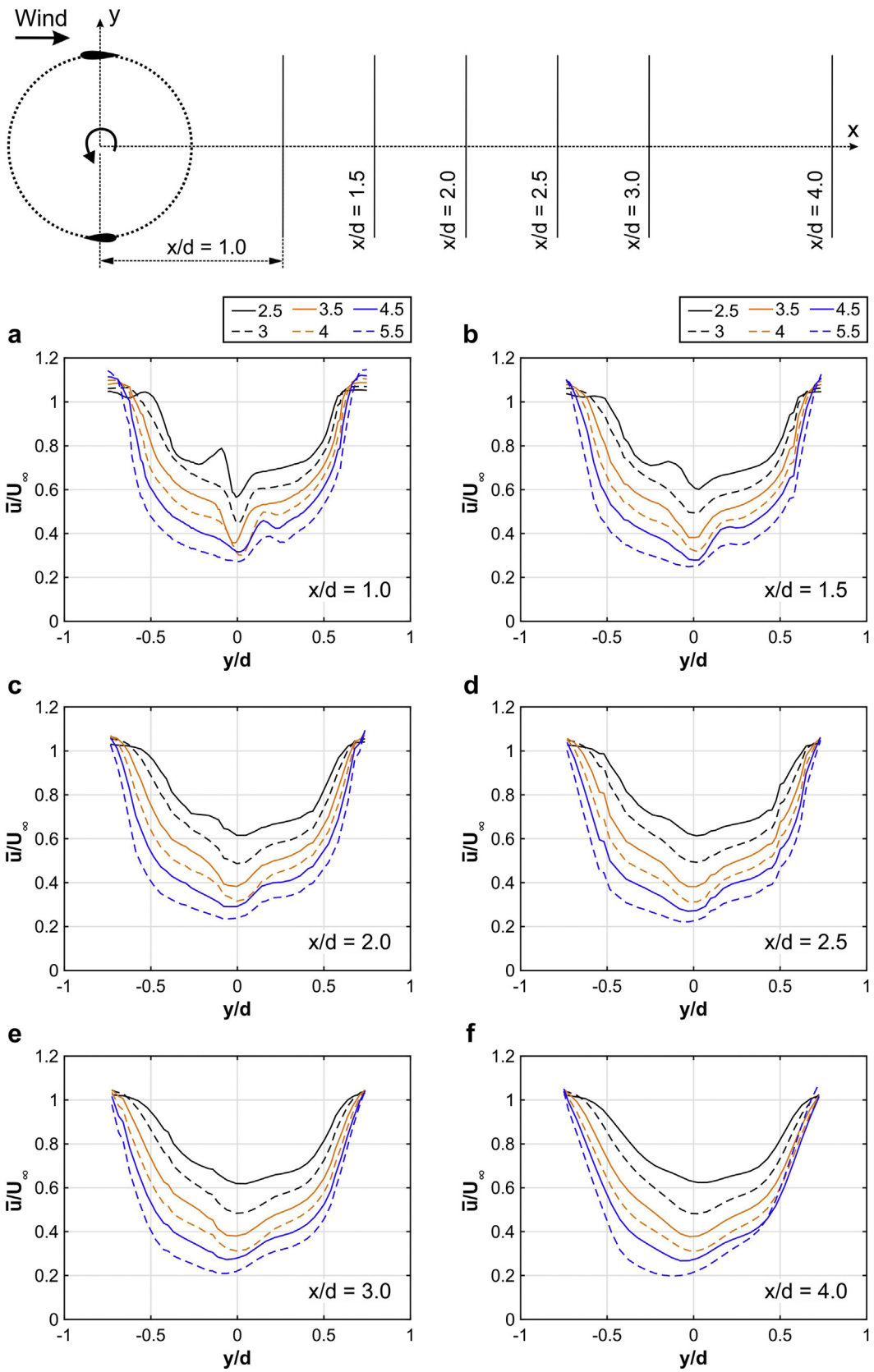

Fig. 11. Time-averaged (over the last turbine revolution) normalized (with freestream velocity) streamwise velocity along lateral lines $-0.75 \leq y/d \leq 0.75$ at several downstream locations for different tip speed ratios. ($Re_c \approx 2.0 \times 10^5$).

Table 4
Turbine wake length vs. tip speed ratio for the reference turbine.

λ	1.5	2.5	3.0	3.5	4.0	4.5	5.5
L_w/d	40	23	19	16	14	13	10

Table 5
Operational parameters to find the optimal λ at different U_∞.

λ	1.2 – 6.0
U_∞ [m/s]	2.3 – 22.3
Ω [rad/s]	11.6 – 204.6
TI [%]	5
Re_c ($\times 10^5$)	0.3 – 4.3

vortex system could be due to variations in angle of attack and/or incoming flow that both simultaneously occur for VAWTs during each revolution. This results in a continuous vortex shedding and the following generation of wake. The strength of the shed vorticity by a single blade can be calculated using Eq. (1) defined as the gradient of circulation per each azimuthal increment. Based on the Kutta–Joukowski theorem [111], a positive value denotes counter-clockwise circulation. Eq. (2) presents a non-dimensional form of Eq. (1). Fig. 10 shows the strength of the shed vorticity during the last turbine revolution for different tip speed ratios. The following observations are made:

- In the turbine fore half, during the upstroke where the circulation around the blade and consequently C_l increase, clockwise vortices (negative sign) are shed. Conversely, during the downstroke where the circulation around the blade and consequently C_l decrease, counter-clockwise (positive sign) vortices are shed. The signs reverse in the turbine aft half.
- The impact of stall on the blade and blade-wake interactions, for $\lambda \leq 3.0$, are aparent as large oscillations in the strength of shed vorticity.
- Decrease of λ increases the strength of the shed vorticity which is in line with the higher slope of C_l-α curve for lower λ. This is clearly shown for $0^\circ \leq \theta \leq 135^\circ$.
- Increase of λ decreases the magnitude of oscillations in the strength of the shed vorticity. This is due to smaller Δα and subsequently more limited separation on the blade. Therefore, for larger λ (> 3.0) where the occurrence of stall is avoided, the variations in the strength of the shed vorticity is mostly due to the unsteadiness in the angle of attack and the incoming flow while for lower λ (≤ 3.0) stall and the blade-wake interactions also have noticeable effects.

$$\frac{\partial \Gamma}{\partial \theta} = -0.5 U_\infty c \frac{\partial C_l}{\partial \theta} \tag{1}$$

$$\frac{2\pi}{c U_\infty} \frac{\partial \Gamma}{\partial \theta} = -\pi \frac{\partial C_l}{\partial \theta} \tag{2}$$

Fig. 11 shows profiles of the time-averaged (over the last turbine revolution) streamwise velocities (normalized with respect to the freestream velocity) along the lateral line, $-0.75 \leq y/d \leq 0.75$, at different downstream locations in the turbine wake with x/d = 1.0, 1.5, 2.0, 2.5, 3.0, 4.0, for various tip speed ratios. It can be seen that:

- For all downstream locations, the velocity deficit in the turbine wake grows as λ increases. This is because the turbine thrust force gets larger when λ increases resulting in further velocity

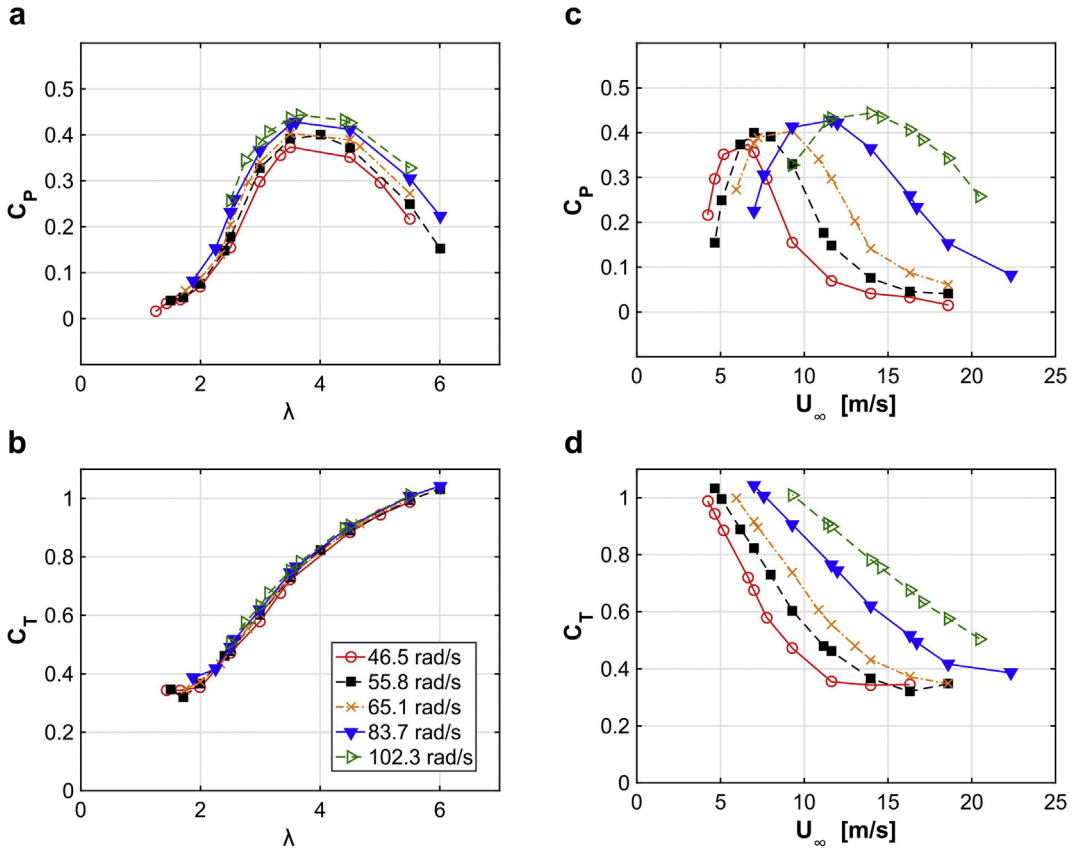

Fig. 12. Power and thrust coefficients versus tip speed ratio and freestream velocity for different fixed rotational velocities.

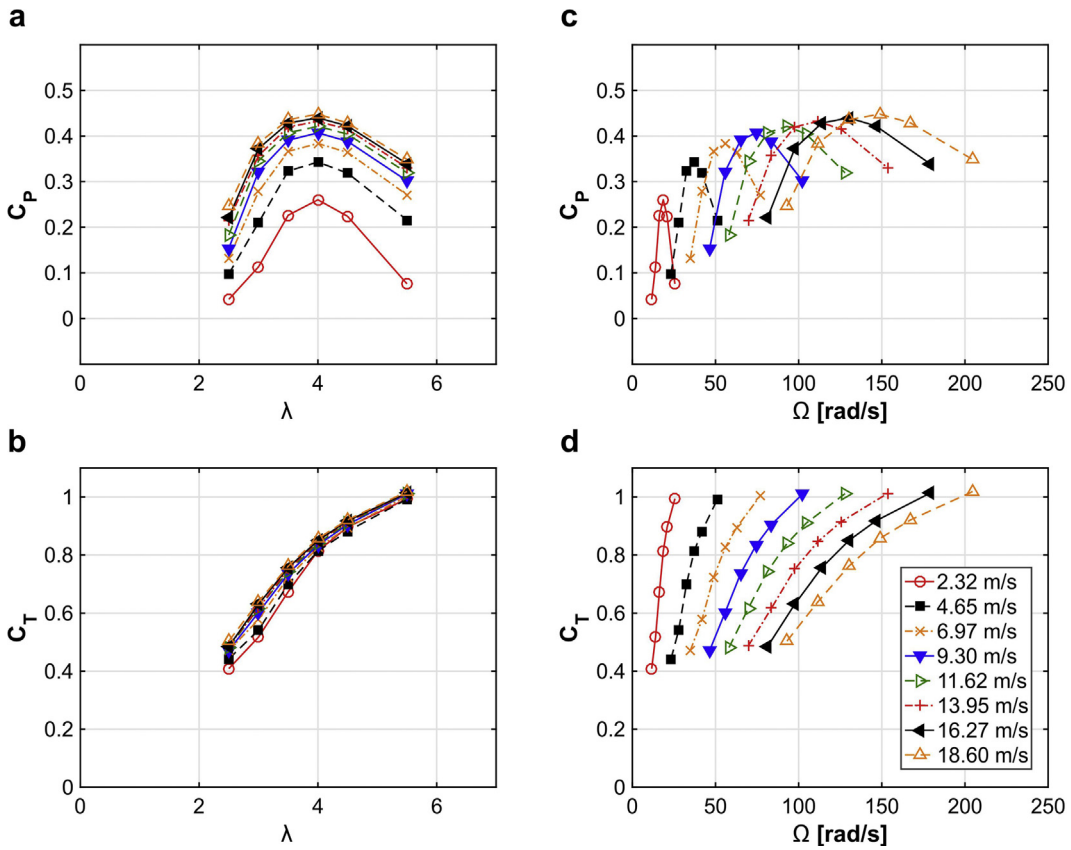

Fig. 13. Power and thrust coefficients versus tip speed ratio and rotational velocity for different fixed freestream velocities.

deceleration (see Fig. 8c). This is in agreement with the experimental observations by Araya and Dabiri [61].

- Increasing λ is found to increase the wake expansion and streamwise asymmetry which is in line with the wind-tunnel measurements by Araya and Dabiri [61].
- The wake self-induction is found to occur for all λ where this is more noticed for higher λ. The wake self-induction refers to reduction in the streamwise velocity as the wake travels downstream. This is consistent with the experimental observations by Tescione et al. [82].
- For $\lambda = 2.5$, the impact of large oscillations, already observed in the strength of the shed vorticity for $220^\circ \leq \theta \leq < 260^\circ$ (see Fig. 10), is also seen in the streamwise velocity for $x/d \leq 1.5$. This fades out as the wake travels further downstream.
- The influence of the shaft is distinguished as a larger velocity deficit at $y/d \approx 0$. This is more pronounced for lower λ values at $x/d < 2.0$, which also fades out as the wake travels further downstream.

Tip speed ratio is also found to significantly influence the length of the turbine wake L_w, which is defined from the turbine center to a downstream location along the turbine centerline, $y/d = 0$, where the normalized velocity magnitude $V/U_\infty = 0.97$. L_w is found to asymptotically decrease from 40d to 10d when λ increases from 1.5 to 5.5 for the reference turbine (see Table 4). The earlier breakdown of the wake for higher λ is attributed to the closer distance between the shed vortices in the wake, which eventually amplifies the wake instabilities and results in an earlier wake structure breakdown. More detailed results on the impact of λ on L_w and comprehensive discussions are provided in Ref. [90]. The trend is in line with the experimental observations for HAWTs [112].

4.4. Optimal tip speed ratio

Unlike HAWTs, VAWTs are currently designed to operate at constant rotational velocity mainly due to simplicity and costs [12,113,114]. This means that for a wide range of freestream velocities, their operation is not optimal and they operate optimally only at a specific wind speed. Two series of simulations are performed for the reference turbine covering a wide range of wind speeds (2.3–22.3 m/s), rotational velocities (11.6–204.6 rad/s) and tip speed ratios (1.2–6.0) in order to investigate the optimal operation of the reference turbine. The two series include simulations at fixed rotational velocities and at fixed freestream velocities. Table 5 lists the operational parameters used to find the optimal tip speed ratio for different freestream velocities.

Fig. 12 shows the turbine power and thrust coefficients versus tip speed ratio and freestream velocity for different fixed rotational velocities $46.5\,\text{rad/s} \leq \Omega \leq 102.3\,\text{rad/s}$. Fig. 13 shows the turbine power and thrust coefficients versus tip speed ratio and rotational velocity for different fixed freestream velocities $2.3\,\text{m/s} \leq U_\infty \leq 18.6\,\text{m/s}$.

At low λ, the turbine has very low C_P. Increasing λ results in a growth of C_P to a maximum value with a high slope. C_P gradually decreases with further increase of λ. This trend is similarly observed at both fixed rotational and freestream velocities, which implies that based on λ three operating regimes for VAWTs are typically defined as follows:

- High wind speed regime: this regime corresponds to low λ where the flow is largely separated on blades at high α (see Section 4.1) and the performance is adversely affected by dynamic stall.
- Optimal regime: this regime associates with where the turbine is producing the maximum C_P.
- Low wind speed regime: this regime refers to high λ where the variations of α on blades are very small, therefore, the blade is operating inefficiently (see Section 4.1).

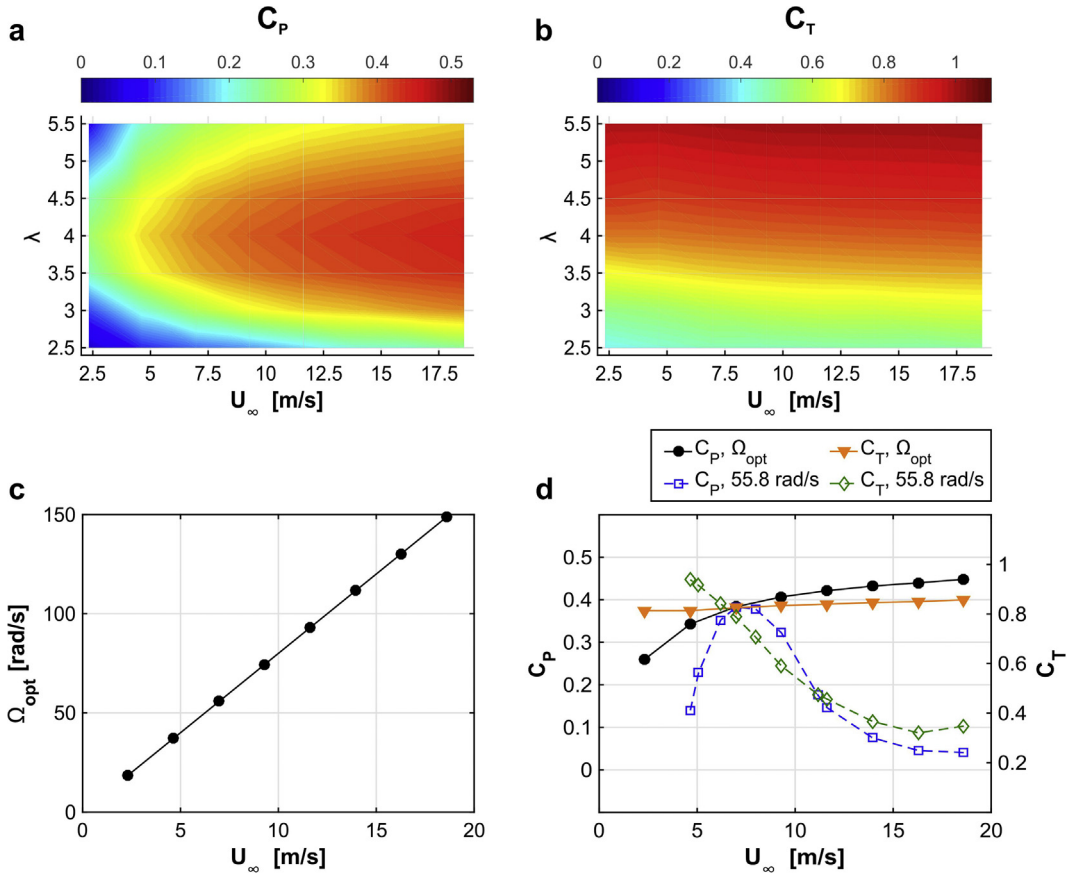

Fig. 14. Contours of coefficients of (a) power and (b) thrust based on 48 simulations described in Table 5; (c) optimal rotational velocity and (d) the power and thrust coefficients corresponding to the optimal λ and fixed Ω of 55.8 rad/s versus freestream velocity.

Table 6
Improvement in C_P due to maintaining optimal λ.

Ω [rad/s]		U_∞ [m/s]								
		4	5	6	7	8	9	10	11	12
46.5	ΔC_P [%]	24	11	5	11	46	124	220	351	549
55.8	ΔC_P [%]	145	63	11	1	4	21	54	122	211
65.1	ΔC_P [%]	168	116	42	8	5	4	13	28	57

Table 7
Operational parameters to study the impact of Re_c.

λ	2.5	3.0	3.5	4.0	4.5	5.5
U_∞ [m/s]	2.3 – 37.2	2.3 – 32.5	2.3 – 27.9	2.3 – 25.0	2.3 – 22.3	2.3 – 18.6
Ω [rad/s]	11.6 – 186.0	13.9 – 195.3	16.3 – 195.3	18.6 – 223.0	20.9 – 200.9	25.5 – 204.6
TI [%]	5	5	5	5	5	5
TI_i [%]	4.42	4.42	4.42	4.42	4.42	4.42
Re_c (× 10^5)	0.3 – 4.1	0.3 – 4.2	0.3 – 4.2	0.3 – 4.2	0.4 – 4.2	0.5 – 4.3

The aforementioned regimes can also be shown when considering the C_P-U_∞ (C_P-Ω) curve (Figs. 12c and 13c):

- At low U_∞ (high Ω), the turbine is performing sub-optimal.
- Increasing U_∞ (decreasing Ω) improves the turbine performance where for each fixed Ω (U_∞), there exists a specific U_∞ (Ω) where the turbine is operating optimally.
- Further increase of U_∞ (decrease of Ω) deteriorates the performance due to the growth of separations on blades and the subsequent stall.

C_T asymptotically grows as λ increases. This occurs at both fixed rotational and freestream velocities. This can also be shown by C_T-U_∞ (C_T-Ω) curves where increasing U_∞ (decreasing Ω) reduces C_T. Increase of C_T by increasing λ is in line with the increase of normal forces on blades shown in Fig. 8b. At high λ due to small α on blades, the generated force is more contributing to thrust force than the tangential force, which is responsible for power generation.

Increasing either the freestream or rotational velocity is found to shift upward the C_P-λ curve. This improvement in turbine performance is attributed to Reynolds number effect which is extensively discussed in Section 5.

To further generalize the findings and to derive the optimal operating condition of the turbine, the results presented in Figs. 12 and 13 are employed to construct contours of C_P and C_T in λ-U_∞ space as shown in Fig. 14a and b. Fig. 14a clearly suggests that to keep the optimal operation of the turbine at different wind speeds, the turbine needs to maintain a constant λ, which is 4.0. Note that the optimal value of λ is dependent on the turbine characteristics and will be different for a turbine of different solidity and/or airfoil shape. Therefore, such analysis will need to be repeated for that case to identify the optimal λ. Based on that, the turbine optimal Ω versus U_∞ is derived and depicted in Fig. 14c. Therefore, Ω needs to increase linearly with U_∞. A comparison of the turbine performance operating at the optimal λ of 4.0 against the operation at a constant Ω, i.e. 55.8 rad/s, is shown in Fig. 14d. Table 6 presents the improvement in C_P due to maintaining the optimal λ compared to turbine operating at fixed Ω of 46.5, 55.8 and 65.1 rad/s. The comparison reveals huge enhancement in C_P for all U_∞. The improvement in C_P would result in large increase in the annual energy production (AEP) which would, therefore, justify the added complexity and cost for a variable-speed VAWT.

The C_T for the turbine operating at the optimal λ is found to stay

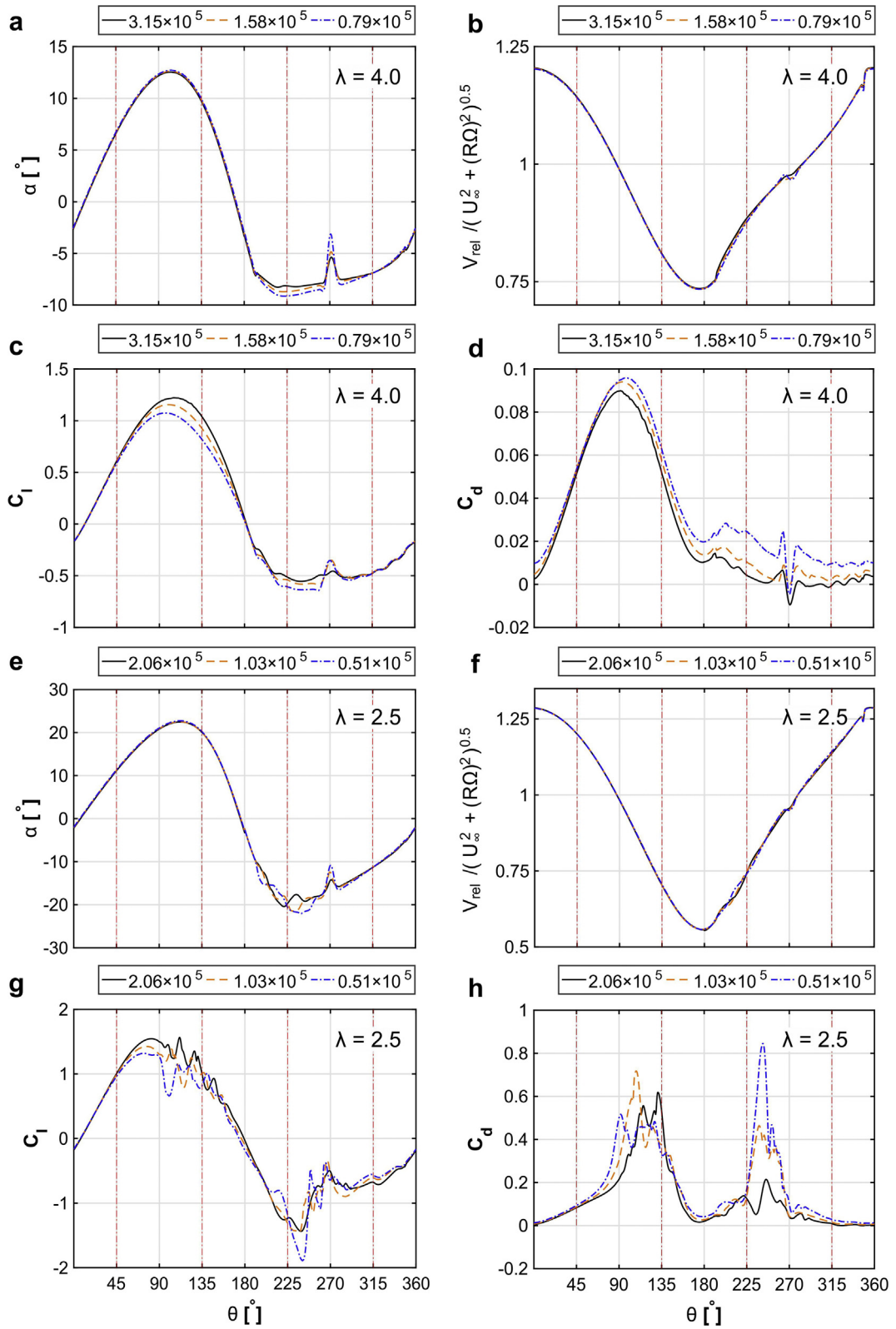

Fig. 15. Variations of experienced angle of attack, normalized relative velocity, lift and drag coefficients during the last turbine revolution for different Re_c at λ: (a–d) 4.0, (e–h) 2.5.

almost constant with small increase due to Reynolds number effects (see Section 5). This can reduce the flapwise fatigue loads on the turbine blades which are caused by the fluctuations in the thrust force. Such fluctuations occur due to the unsteady incoming flow.

5. Impact of Reynolds number

The current section investigates the impact of Re_c, based on the blade chord length, on the dynamic loads on turbine blades, turbine performance and wake at different tip speed ratios. A wide range of

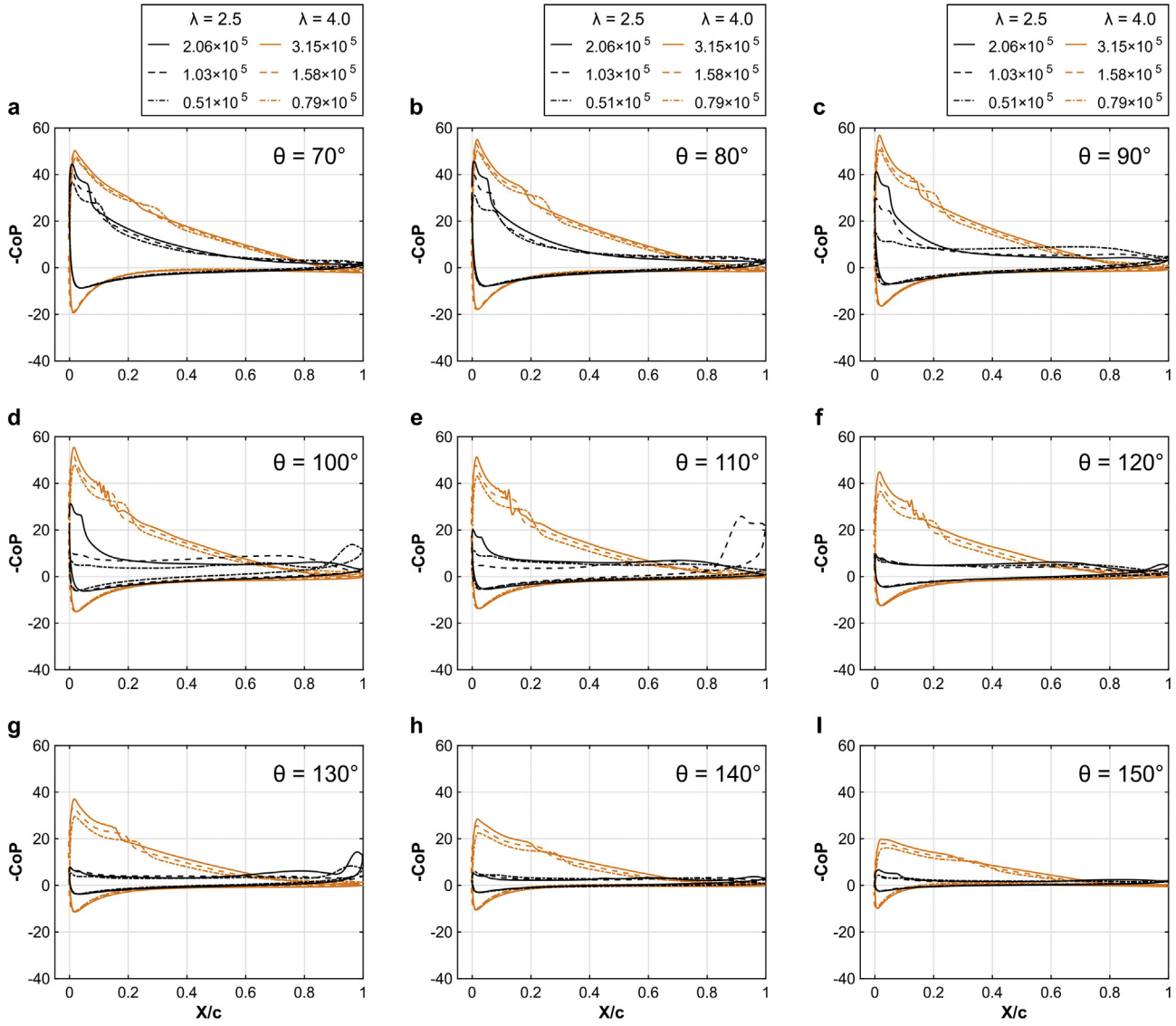

Fig. 16. Pressure coefficient (CoP) over the blade during the last turbine revolution for different Re_c at azimuthal positions set in Fig. 5 for λ = 2.5 and 4.0. X/c represents the dimensionless chordwise position along the blade.

$Re_c = 0.3 \times 10^5 - 4.3 \times 10^5$ is considered where the range covers the values corresponding to small- to medium-scale urban VAWTs [12]. The turbulence intensity and the reduced frequency are kept the same as in the reference case. The other main operational parameters are presented in Table 7. An overall analysis is performed for $2.5 \leq \lambda \leq 5.5$ covering low to moderately high tip speed ratios while a more detailed analysis focuses on the optimal λ of 4.0 and λ = 2.5, where the blade is in dynamic stall. It should be noted that the two selected λ will cover the two distinctive turbine operation regimes based on the flow physics: the former corresponds to the regime when the flow is mostly attached while the latter corresponds to the regime that includes strong separation from the blades. Therefore, these two deserve a dedicated analysis.

5.1. Loads on blades

The variations of α, V_{rel}, dynamic C_l and C_d during the last turbine revolution for different Re_c are compared in Fig. 15 for λ = 4.0 and λ = 2.5. The Re_c ranges between 0.79×10^5 –3.15×10^5 and 0.51×10^5 –2.06×10^5 for λ = 4.0 and 2.5, respectively.

For λ = 4.0 (optimal performance), in the turbine fore half:

- Re_c has a negligible influence on α during the upstroke ($0^\circ \leq \theta \leq 45^\circ$).
- Normalized V_{rel} is Re-independent.
- During the upstroke, Re_c has negligible effect on C_l, especially for $Re_c \geq 10^5$.
- Near $C_{l,max}$ and during the downstroke, $45^\circ < \theta \leq 180^\circ$, increasing Re_c increases C_l and $C_{l,max}$, slightly postpones $\alpha_{cl,max}$ to higher θ and marginally reduces C_d. Given the constant value of α for different Re_c, these are associated to the delay in trailing-edge separation, which will be discussed later in this section. This is in agreement with earlier studies on airfoils in similar Re regime [70].
- C_l is more sensitive to Re_c for $Re_c \leq 1.58 \times 10^5$. This threshold is consistent with the findings for static airfoils reported by Lissaman [74].

In the turbine aft half:

- Re_c has noticeable influence on α and C_l mainly in two regions, (i) $235^\circ \leq \theta \leq 265^\circ$ where the flow has already slightly lower velocity due to the improved blade performance and more efficient energy extraction (less energy is remained in the flow) at higher Re_c. The lower velocity results in lower α and C_l for higher Re_c, (ii) $\theta \approx 270^\circ$

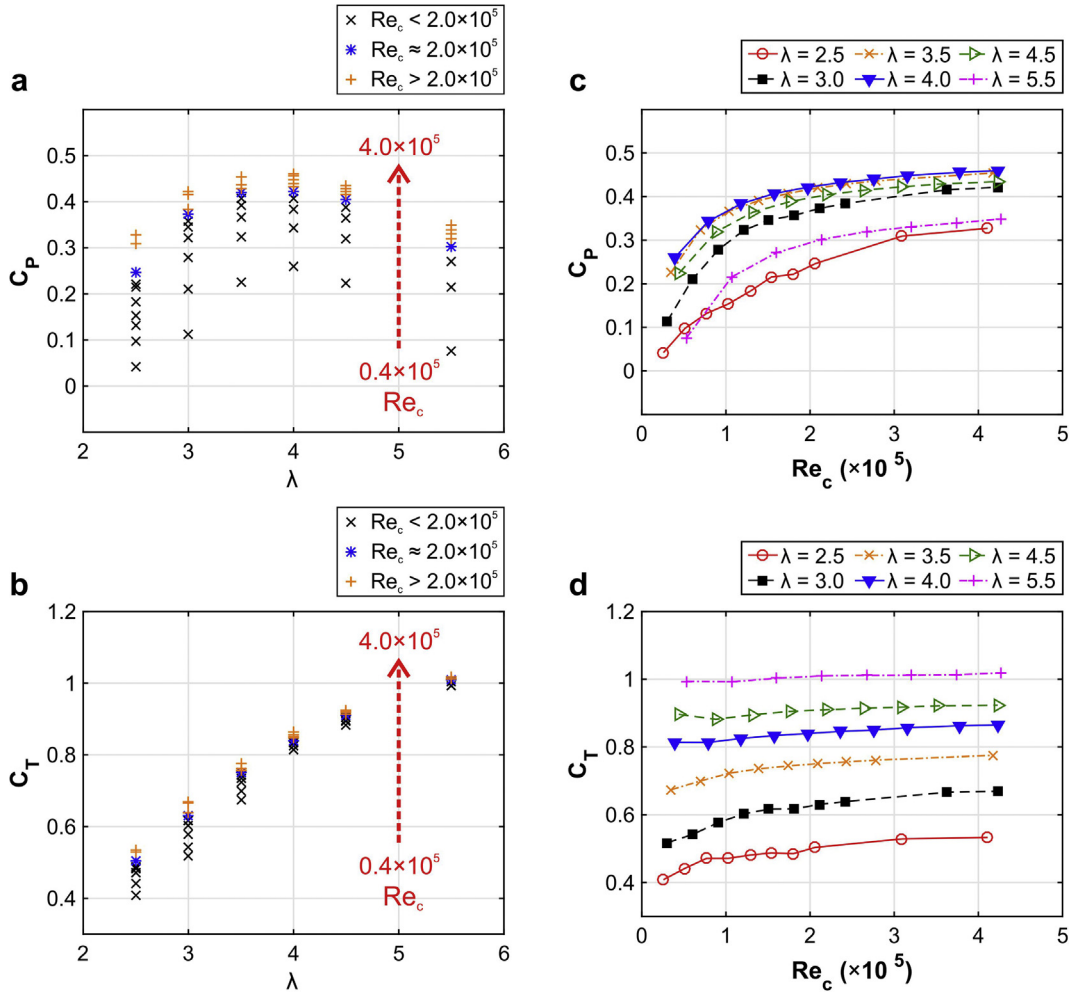

Fig. 17. Power and thrust coefficients versus tip speed ratio ($2.5 \leq \lambda \leq 5.5$) and chord-based Reynolds number ($0.4 \times 10^5 < Re_c < 4.0 \times 10^5$).

where increasing Re_c noticeably diminishes the sudden change in all parameters in the shaft wake. This is due to the strong Reynolds number effects on shaft, where increasing Re significantly delays the separation and reduces the wake width. Note that the Re corresponding to the shaft is defined based on its diameter and solely the incoming flow, which therefore, will be significantly lower than Re_c. An extensive discussion on the effect of the turbine shaft for VAWTs is provided by Rezaeiha et al. [55].

- Increasing Re_c is found to significantly reduce C_d, especially for $Re_c \leq 1.58 \times 10^5$. Note that given the small variations of α, the flow on the blade is mostly attached in this region. For attached flows on flat plates and airfoils, increasing Re effectively reduces the turbulent shear stress, and consequently the skin friction drag, while such an effect becomes less strong by increasing Re above 10^5 [72].

For $\lambda = 2.5$ (dynamic stall), similar observations as the optimal λ are made while the following points are also noteworthy. In the turbine fore half, the delay in stall by increasing Re_c is evident from the postponement of $C_{d,max}$. While increasing Re_c visibly increases $C_{l,max}$, no monotonic trend is found for $C_{d,max}$. The complexities associated with the impact of Re_c on dynamic stall has also been already reported by Singleton and Yeager Jr. [115]. In the turbine aft half, for $235^\circ \leq \theta \leq 265^\circ$, increasing Re_c is found to reduce fluctuations in α, C_l and C_d which occurs due to the blade-wake interactions as explained in Section 4.1.

Plotting the lift and drag coefficients versus angle of attack, which for brevity is not shown here, implies that the hysteresis in dynamic loads is marginally increased by Re_c prior to stall, i.e. $\lambda = 4.0$, while is weakly influenced by Re_c post-stall, i.e. $\lambda = 2.5$. This is in line with the experimental results of Bousman [116], which showed weak Re-dependency for dynamic stall at Re_c $1 \times 10^5 - 2.5 \times 10^5$.

The pressure coefficients on the blade are shown in Fig. 16. Note that in this figure the azimuthal positions, and λ and Re_c are corresponding to those values already employed in Figs. 5 and 15, respectively. It can be seen that:

- An increase in Re_c promotes laminar-to-turbulent transition on the blade suction side. This is in agreement with the studies on airfoils and flat plates [72,74,103]. Similar to observations in Section 4.1, the transition occurs earlier and the length of LSB is shorter for lower λ due to higher values of α.
- An increase in Re_c delays the separation on the blade. For $\lambda = 2.5$, at $\theta > 90^\circ$ the blade has already stalled for the lowest Re_c of 0.51×10^5 while this occurs at $\theta > 110^\circ$ for the highest Re_c of 2.06×10^5. The delay in separation is associated to the promotion in laminar-to-turbulent transition. The turbulent boundary layer has higher energy, thus, is more resistant to adverse pressure gradient and will separate later.
- Increasing Re_c also slightly increases the pressure difference on the blade which explains the improvement in C_l shown in Fig. 15. The increment in pressure difference is found to be present both in laminar and turbulent regions of the blade. This can be associated to the reduction in skin friction by increasing Re_c [74].

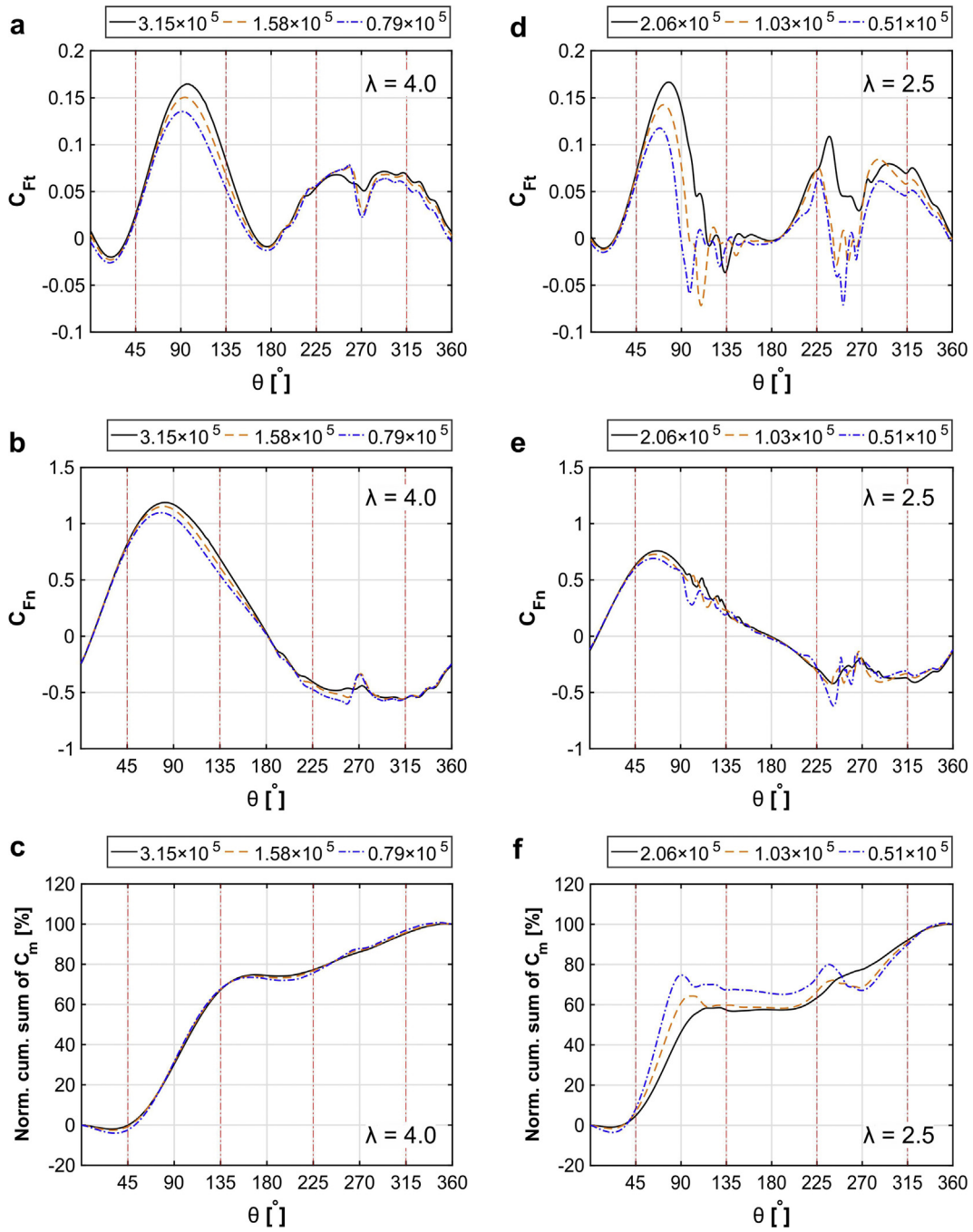

Fig. 18. Coefficients of tangential and normal forces and the normalized cumulative sum of the moment coefficient during the last turbine revolution for different Re_c for (a–c) $\lambda = 4.0$ and (d–f) $\lambda = 2.5$.

5.2. Turbine performance

Fig. 17a and b show the turbine power and thrust coefficients versus tip speed ratio for different freestream chord-based Reynolds numbers $0.4 \times 10^5 \leq Re_c \leq 4.0 \times 10^5$. The range is selected corresponding to very small to moderate size VAWTs operating in the urban environment. Increasing Re_c is found to significantly improve the turbine performance while the optimum λ is Re-independent. The enhancement in C_P at $\lambda = 2.5$ (dynamic stall) and the optimal λ of 4.0 is 682% and 77%, respectively, when Re_c increases from approximately 0.4×10^5 to 4.0×10^5.

As already shown in Section 5.1, increasing Re_c results in two effects on the blade, i.e. increase in the pressure difference and the promotion of laminar-to-turbulent transition which eventually delays the separation. For a given geometrical design and operating condition, Re_c will be fixed. Therefore, if any method can mimic the two effects of Re_c, it could also significantly improve the turbine performance. Flow control methods have emerged as promising options to introduce the two effects. For example, circulation control methods can be employed to increase the pressure difference on airfoils [117]. Separation control methods have also been shown to successfully delay the blade stall to higher α [103].

By increasing λ, the effect of Re_c on C_T becomes less pronounced. As Re_c increases from 0.4×10^5 to 4.0×10^5, C_T increases by 30.5% and 4.7% at $\lambda = 2.5$ and 4.0, respectively.

In order to further clarify the impact of Reynolds number, the

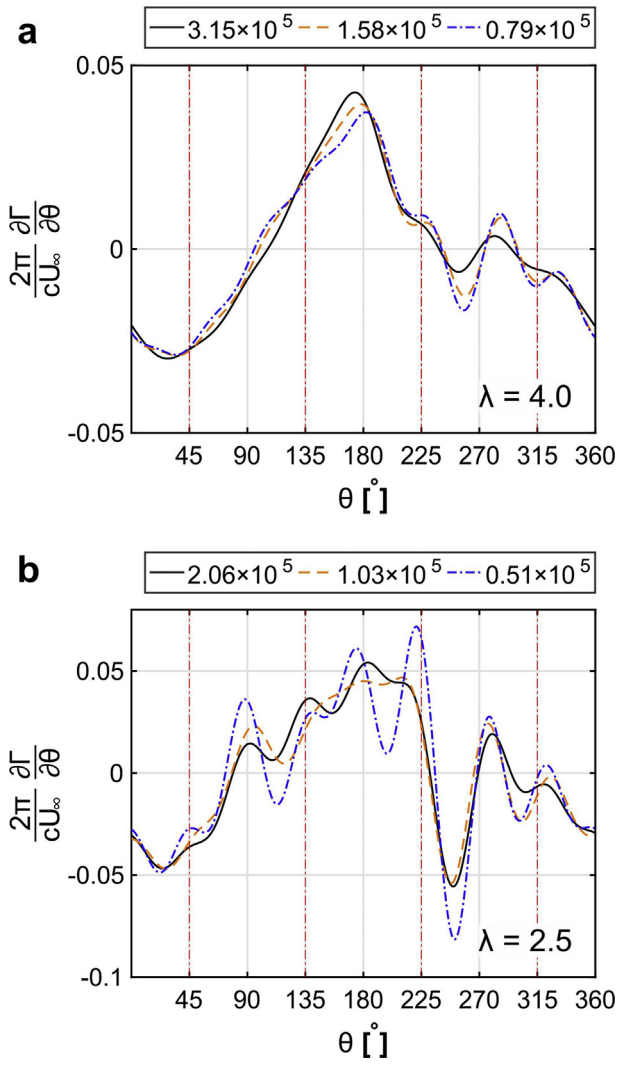

Fig. 19. Shed vorticity by a single blade during the last revolution for different Re_c at λ: (a) 4.0, (b) 2.5. Positive values denote counter-clockwise circulation based on the Kutta–Joukowski theorem [111].

turbine power and thrust coefficients versus Re_c for different tip speed ratios $2.5 \leq \lambda \leq 5.5$ are illustrated in Fig. 17c and d. It can be seen that increasing Re_c asymptotically improves C_P. The asymptotic trend could be explained as follows: as Re_c increases and transition onset shifts upstream toward the leading edge, at one point flow on a large part of the blade is already turbulent and further promotion of the transition will have negligible effect. The asymptotic trend is in agreement with the experimental observations by Bachant and Wosnik [65] for hydro turbines. The results of the present study reveal that for Re_c up to 4×10^5, the turbine performance is still Re-dependent which is in contrast with the results of Bachant and Wosnik [65] where they reported a Re-independent performance for $Re_c \geq 2 \times 10^5$. The difference could be associated to the large difference in turbine solidity between the two studies. In the present study, the turbine has a low solidity of 0.12 while in the experiment they had a large solidity of 0.42 (which is more relevant for hydro turbines). The comparatively small impact of Re_c on C_T is also clearly seen in Fig. 17d. For $\lambda \geq 4.0$, C_T is almost Re-independent for the whole range studied. For $\lambda < 4.0$, the Re-independence regime is limited to $Re_c > 2 \times 10^5$.

Fig. 18 compares the instantaneous tangential C_{Ft} and normal C_{Fn} force coefficients on blades and the normalized cumulative sum of instantaneous moment coefficient C_m during the last turbine revolution for the optimal λ of 4.0 and $\lambda = 2.5$ (dynamic stall) for different Re_c. For $\lambda = 4.0$, Re_c varies between 0.79×10^5 and 3.15×10^5. For $\lambda = 2.5$, the Re_c variation is from 0.51×10^5 to 2.06×10^5. For the optimal λ of 4.0, the following observations are made:

- Increasing Re_c is found to significantly increase the tangential loads on turbine blades in the turbine fore half. The increment was already shown to be due to the promotion in laminar-to-turbulent transition, delay in separation and reduction in drag for higher Re_c.
- Increasing Re_c improves the loss in tangential loads in the shaft wake $\theta \approx 270°$. As discussed, the improvement corresponds to the delay in separation on the shaft and the consequent reduction in shaft wake by increasing Re.
- Normal loads are found to be less sensitive to Re_c. In the turbine fore half, normal loads increase by increasing Re_c, while the magnitude of increment is smaller than the tangential loads. Similar observation is made in the shaft wake where the reduction in normal loads is comparatively small.
- Re_c is found not to alter the contribution of different turbine quartiles to the total power production.

For $\lambda = 2.5$ (dynamic stall), it can be seen that:

- The sudden drop in tangential loads in the turbine fore half occurs later for higher Re_c. This prompts the delay in stall.
- A reduction in tangential and normal load fluctuations, by increasing Re_c is noticeable. This occurs due to stall in the turbine fore half and the blade-wake interactions in the turbine aft half.
- Unlike the optimal λ, increasing Re_c notably affects the contribution of different quartiles to the total power production where the contribution of the upwind quartile lessens and that of the downwind quartile increases. This is associated to the significant influence of Re_c on delaying the stall and remarkably diminishing the strength of shed vorticity from the blades, thus weaker blade-wake interactions at higher Re_c (see Section 5.3). As a result, at higher Re_c, the downstream region is still capable of extracting energy from the flow and contributing to the total power.

5.3. Turbine wake

Fig. 19 shows the strength of the shed vorticity by a single blade during the last turbine revolution for the $\lambda = 4.0$ (optimal value) and 2.5 (dynamic stall). It can be see that at the optimal λ of 4.0, the strength of the shed vorticity by a single blade is insignificantly affected by Re_c. Small differences by increasing Re_c correspond to three regions: (i) delay in separation on the blade in the turbine fore half; (ii) consequent reduction in fluctuations of the strength of the shed vorticity due to smaller blade-wake interactions in the turbine aft half; and (iii) diminishing of the impact of the shaft wake.

At $\lambda = 2.5$ (dynamic stall), the influence of Re_c is apparent in the same three regions while the impact is much more pronounced, especially when increasing Re_c from 0.51×10^5 to 1.03×10^5 where stronger vortex shedding and larger instability in the strength of the shed vortices are found to occur at the lower Re_c. This is in agreement with the experimental results by Yoon et al. [118].

Fig. 20 presents the time-averaged (over the last turbine revolution) streamwise velocity (normalized with respect to the freestream velocity) along the lateral line, $-0.75 \leq y/d \leq 0.75$, at different downstream locations in the turbine wake with x/d = 1.0, 1.5, 2.0, 2.5, 3.0, 4.0, for $\lambda = 4.0$ (optimal) and 2.5 (dynamic stall) at various Re_c are shown in. It can be seen that:

- The turbine wake mean velocity profile is much less sensitive to Re_c than λ.
- The sensitivity of the wake mean velocity to Re_c does not reduce with traveling further downstream from x/d = 1.0 to 4.0.
- The velocity deficit and the mean velocity profile in the wake of the

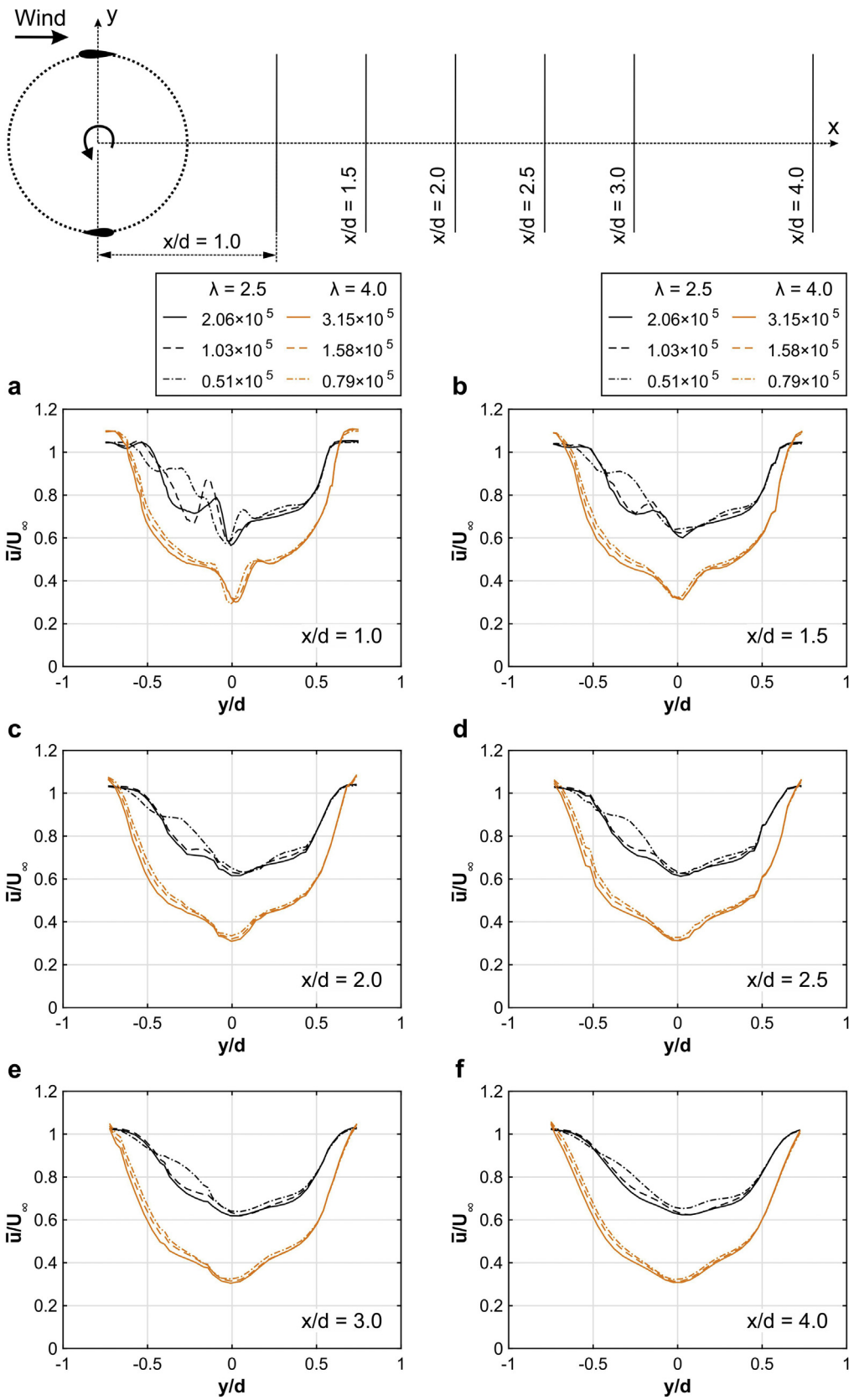

Fig. 20. Time-averaged (over the last turbine revolution) normalized (with freestream velocity) streamwise velocity along the lateral line $-0.75 \leq y/d \leq 0.75$ at several downstream locations for different Re_c at $\lambda = 2.5$ and 4.0.

Table 8
Operational parameters to study the impact of freestream turbulence.

λ	2.5	3.0	3.5	4.0	4.5	5.5
U_∞ [m/s]	9.3	9.3	9.3	9.3	9.3	9.3
Ω [rad/s]	46.5	55.8	65.1	74.4	83.7	102.3
TI [%]	0 – 30	0 – 30	0 – 30	0 – 30	0 – 30	0 – 30
Re_c ($\times 10^5$)	1.03	1.21	1.39	1.58	1.76	2.14

Table 9
Incident total turbulence intensities.

TI [%]	0	5	10	15	20	25	30
TI_i [%]	1e-6	4.42	7.99	11.01	13.64	15.98	18.09

VAWT are Re-dependent within the range studied both for λ = 4.0 and = 2.5. For HAWT, Re-independency for the wake mean velocity is found to occur already at an approximate blade tip Re_c of 2.0×10^4 [119].

- Increasing Re_c increases the velocity deficit for x/d > 1.0. This corroborates the observations by Bachant and Wosnik on hydro turbines [65].
- Increasing Re_c expands the turbine wake. Similar observations are reported for HAWTs by McTavish et al. [120].
- The influence of Re_c is more prominent for λ = 2.5, compared to λ = 4.0, and the impact is larger for Re_c increasing from 0.51×10^5 to 1.03×10^5. This is consistent with the comparatively large impact of Re_c on the strength of the shed vorticity for the lower λ at the same Re_c as shown in Fig. 19. As the turbine wake is generated by the shed vorticity from the blades, therefore, the larger influence of the Re_c on the strength of the shed vorticity will also result in a larger difference in the velocity profiles in the wake.
- For λ = 2.5, at downstream positions x/d < 2.0, the impact of the local blade aerodynamics (vortex shedding due to stall on blades) is strongly distinguished as fluctuations in the mean velocity profile in y/d < 0. The local blade effect fades away as the wake travels further downstream.

The above findings highlight the facts that (i) there exist important differences in Re-dependency of wake characteristics for VAWTs and HAWTs; (ii) in the study of array of reduced-scale VAWTs, Re-dependency of the wake mean velocity and turbulence intensity needs special attention to avoid wrong conclusions for the full-scale turbines.

6. Impact of turbulence intensity

In this section, the impact of freestream turbulence intensity on the dynamic loads on blades, the turbine performance and the wake is systematically investigated. Table 8 lists the operational parameters employed. TI is selected to vary within 0 to 30%, covering a wide range from very low values relevant to low turbulence wind tunnels to moderately high turbulence in the real operating conditions such as urban environments. An overall analysis is performed for $2.5 \leq \lambda \leq 5.5$ covering low to moderately high tip speed ratios while a more detailed analysis focuses on the optimal λ of 4.0 as well as λ = 2.5 where the blade is in dynamic stall. Table 9 presents the incident-flow total turbulence intensities for all the cases. The reduced frequency is kept the same as the reference case.

6.1. Loads on blades

Fig. 21 compares the variations of α, V_{rel}, dynamic C_l and C_d during the last turbine revolution for different TI for λ = 4.0 (optimal) and λ = 2.5 (dynamic stall). For λ = 4.0, the following observations are made:

- α is found not to be affected by TI except in the shaft wake where the magnitude of the sudden change in α abates by increasing TI. This is because increasing TI promotes laminar-to-turbulent transition on bluff bodies [121], which consequently delays the flow separation and reduces the shaft wake width [55].
- At TI = 0%, fluctuations are present in both C_l and C_d which could be associated to the long laminar separation bubble (LSB) existing on the airfoil suction side [109]. Increasing TI damps out such load fluctuations.
- In the turbine fore half, very small differences in C_l are observed for TI = 5% and 30%.
- In the turbine fore half, C_d is highest for TI = 30%. In the turbine aft half, C_d is higher for TI = 30% compared to 5% while strong fluctuations, due the blade-wake interactions and shaft wake, are present for TI = 0%.

For λ = 2.5 (dynamic stall), it can be seen that:

- Fluctuations of α corresponding to the blade-wake interactions downstream of the stall region, already identified in Section 4.1, reduce as TI increases.
- Increasing TI remarkably reduces the load (C_l and C_d) fluctuations due to the stall, the blade-wake interactions and the shaft wake where the difference is much more pronounced from TI of 0% to 5%.
- In contrary to λ = 4.0, increasing TI notably reduces C_d where the minimum C_d corresponds to TI = 30%.
- The minimum $C_{d,max}$ occurring due to the stall and the blade-wake interactions occurs at TI = 30%.
- By increasing TI, stall is delayed. This is apparent from the postponement in $C_{d,max}$ in the turbine fore half.
- $C_{l,max}$ is found not to be affected by TI.

In addition, plotting the lift and drag coefficients versus angle of attack, which for brevity is not shown here, implies that the asymmetry (hysteresis) in the dynamic loads is barely influenced by TI.

The pressure coefficients on the blade are compared in Fig. 22. The following observations are made:

- Similar to observations in Sections 4.1 and 5.1, the transition occurs earlier and the length of LSB is shorter for lower λ due to higher values of α.
- At TI = 0%, a long LSB is present, where the length of the bubble is shorter for λ = 2.5 due to higher α, which is thought to be causing the notable load fluctuations shown in Fig. 21.
- Increasing TI from 0 to 5% significantly decreases the length of LSB. The reduction in the bubble length has been experimentally shown to be associated to the stronger velocity fluctuations, at higher TI, entering the separated boundary layer which tends to reattach the boundary layer and close the bubble [122].
- At TI = 30%, bypass transition occurs for all cases for λ = 4.0. This is limited to θ < 90° and > 130° for λ = 2.5. While for other θ, an early transition within a short LSB at 0 < X/c < 0.1 happens.
- For λ = 2.5 (dynamic stall), the delay in stall by increasing TI is clearly visible. At TI = 0%, the blade stalls at θ = 80°. This is postponed for θ = 100° at TI = 5%. This is further postponed at TI = 30% where separation extends over almost 90% of the blade at θ = 120°.
- For the optimal λ = 4.0 where the flow is mostly attached, TI = 0% has the minimum pressure difference on the blade. A slight increase of pressure difference on the blade by increasing TI from 5 to 30% is present for θ > 100°.

6.2. Turbine performance

Fig. 23 shows C_P and C_T versus λ for 0% ≤ TI ≤ 30% and versus TI for $2.5 \leq \lambda \leq 5.5$. It can be seen that C_P is strongly sensitive to TI for all

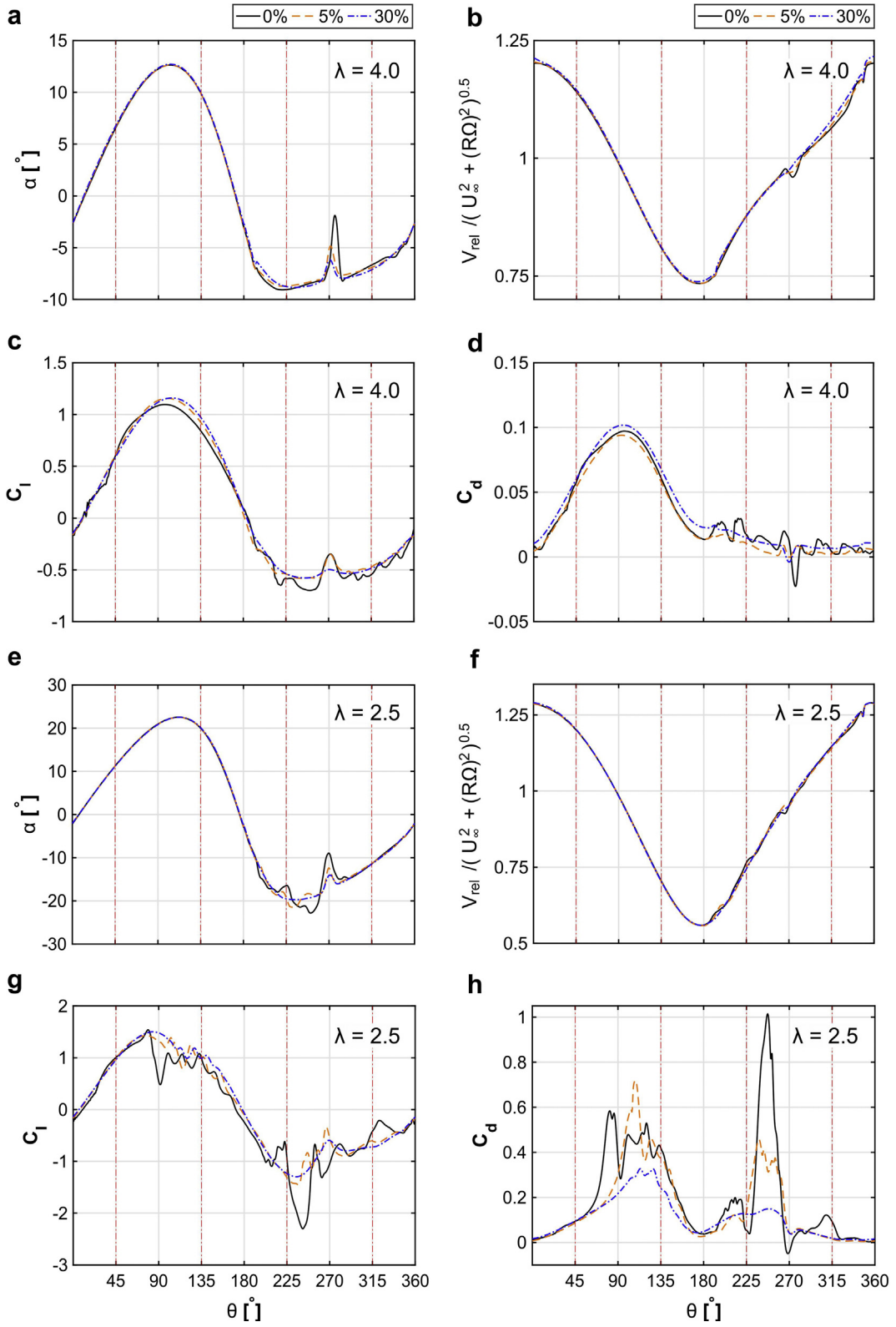

Fig. 21. Variations of experienced angle of attack, normalized relative velocity, lift and drag coefficients during the last turbine revolution for different TI at λ: (a–d) 4.0, (e–h) 2.5.

λ. For low tip speed ratios (λ ≤ 3.0), the sensitivity for TI < 10% is substantial while it quickly decreases for 10% ≤ TI ≤ 30%. Within the studied range of TI, this sensitivity becomes comparatively small for moderate to high tip speed ratios, 3.5 ≤ λ ≤ 4.5, while again increases for higher λ of 5.5. The optimum λ has a small dependence on TI where it slightly decreases from 4.0 to 3.5 by increasing TI from 0% to 30%.

For λ = 2.5, where the flow is strongly separated and dynamic stall is present, increasing TI from 0% to 30% dramatically improves the turbine performance (249%). The improvement is shown to be associated with the promotion in laminar-to-turbulent transition and

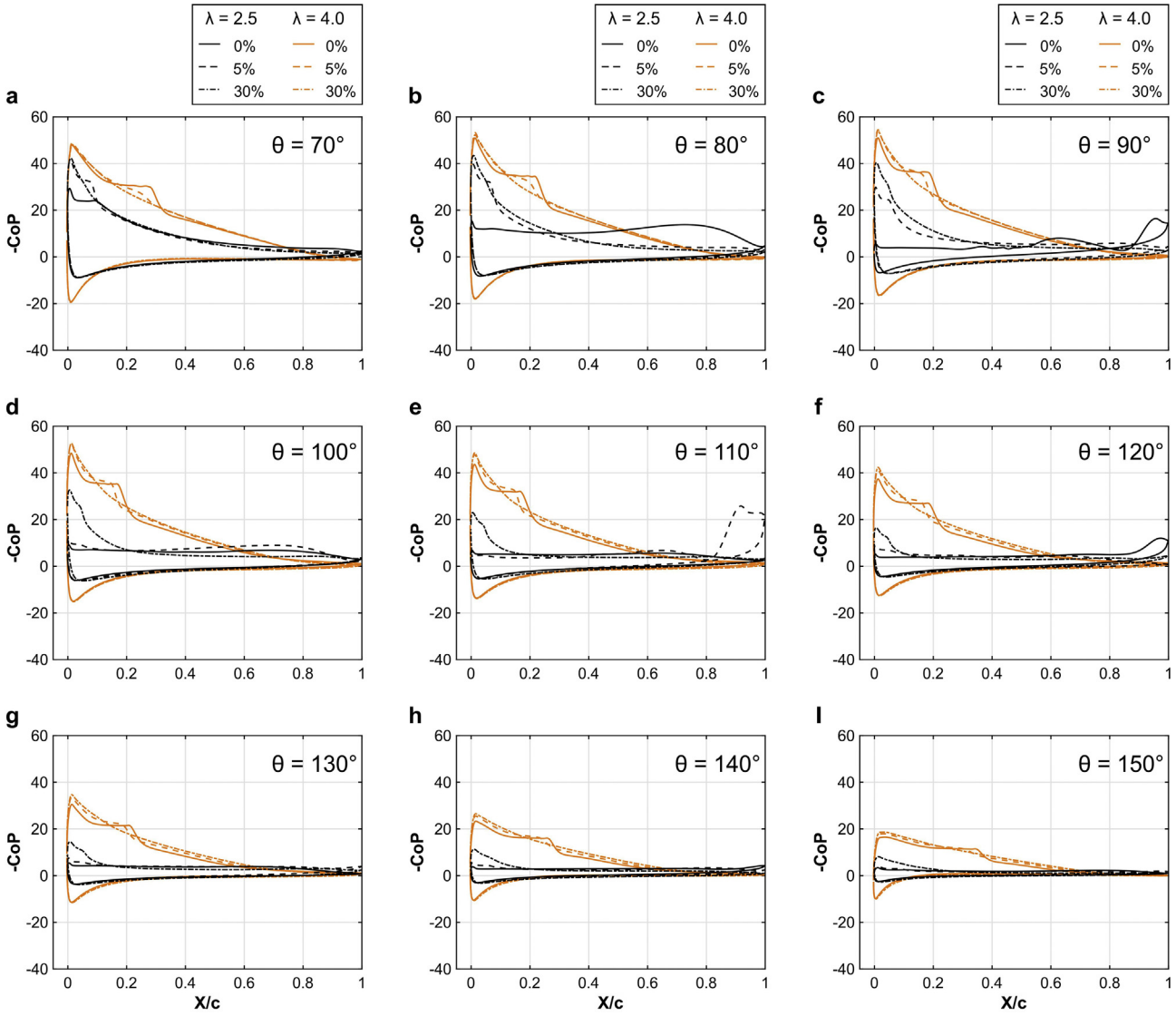

Fig. 22. Pressure coefficient (CoP) over the blade during the last turbine revolution for different TI at azimuthal positions set in Fig. 5 for λ = 2.5 and 4.0. X/c represents the dimensionless chordwise position along the blade.

considerable delay in stall on blade (see Section 6.1).

For λ > 2.5, where the blade is operating prior or near stall, an initial increase of TI from 0% improves the C_P by promoting laminar-to-turbulent transition (happening within a shorter LSB) and increasing the pressure difference on the blade. There exists an optimal TI which grants the maximum C_P. The optimal TI is 15% and 10% for λ = 3.0 and 3.5, respectively, while this reduces to TI = 5% for λ ≥ 4.0. The optimal C_P compared to that of TI = 0% is 87%, 25%, 7%, 6% and 7% higher for λ = 3.0, 3.5, 4.0, 4.5 and 5.5, respectively. This highlights significant influence of TI especially for TI ≤ 15%. Further increase of TI deteriorates the C_P due to massive increase of C_d as a result of large growth of skin friction in the attached boundary layer along the blade. For the optimal λ = 4.0, the maximum C_P, which occurs at TI = 5%, drops by 9% at TI = 30%. The reduction grows to 23% for λ = 5.5. The comparatively high reduction at λ = 5.5 could be explained as for higher λ, flow is attached over a larger part of the blade, therefore, friction drag is playing a more important role. For λ ≥ 4.0, C_P at TI = 30% is lower than that of TI = 0%. C_T can be considered almost TI-independent.

Fig. 24 presents the instantaneous tangential C_{Ft} and normal C_{Fn} force coefficients on the blades and the normalized cumulative sum of instantaneous moment coefficient C_m during the last turbine revolution for the optimal λ of 4.0 and λ = 2.5 (dynamic stall) for different TI values. For the optimal λ of 4.0, it can be seen that:

- Increasing TI from 0% to 5% improves the tangential loads in the turbine fore half while further increase of TI to 30% decreases the tangential loads. The explanation is provided in Section 6.1.
- The loads in the shaft wake behave differently where TI = 30% shows the least reduction in loads. This is because the flow over a bluff body, namely the shaft, is driven by large separation and friction drag plays a minimal role to the total drag. Therefore, increase of TI delays the separation and reduces the shaft wake, which consequently improves the tangential loads in this region.
- Normal loads are less sensitive to TI. In the turbine fore half, the normal loads slightly increase due to higher TI, especially during the downstroke while the reverse occurs in the turbine aft half.
- The contribution of different quartiles are minimally affected by TI (Fig. 24c).

For λ = 2.5 (dynamic stall) it can be observed that:

- Increasing TI monotonically improves the tangential loads in dynamic stall by dramatically delaying the stall. This is clearly

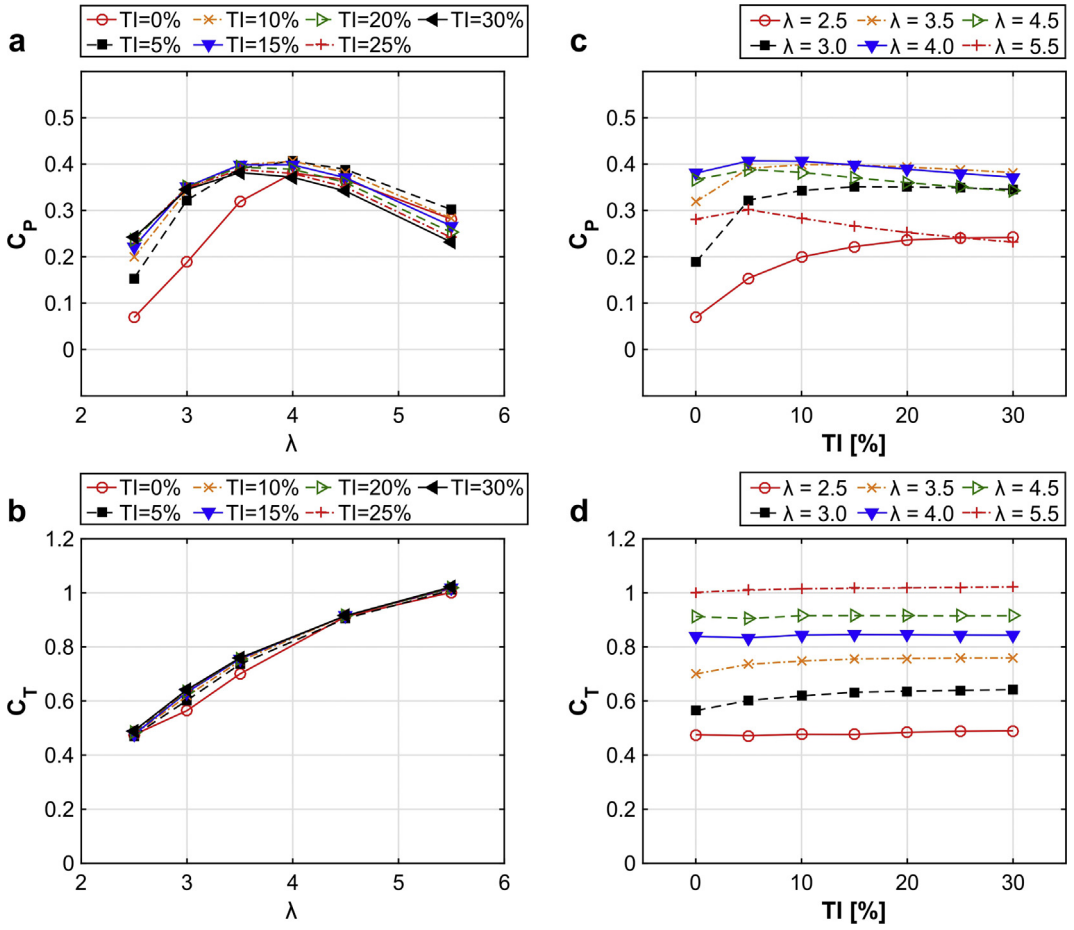

Fig. 23. Power and thrust coefficients versus tip speed ratio ($2.5 \leq \lambda \leq 5.5$) and turbulence intensity ($0\% < TI < 30\%$).

distinguished from the postponement in the abrupt drop in tangential loads for higher TI.
- Increasing TI significantly diminishes the fluctuations in tangential and normal loads.
- Due to the considerable changes in the flow by delaying stall in the turbine fore half, the contribution of different quartiles to the total power production is altered.

6.3. Turbine wake

Fig. 25 shows the strength of the shed vorticity by a single blade during the last turbine revolution for $\lambda = 4.0$ (optimal value) and 2.5 (dynamic stall). It can be seen that:

- At the optimal λ of 4.0, increasing TI from 0 to 5% diminishes the fluctuations in the strength of the shed vorticity while further increase of TI yields to less significant impact.
- At $\lambda = 2.5$, the similar observation is made while the impact of TI in reducing the fluctuations in the strength of the shed vorticity is much more pronounced.

Fig. 26 indicates the time-averaged (over the last turbine revolution) streamwise velocity (normalized with respect to the freestream velocity) along the lateral line, $-0.75 \leq y/d \leq 0.75$, at different downstream locations in the turbine wake with $x/d = 1.0, 1.5, 2.0, 2.5, 3.0, 4.0$, for $\lambda = 4.0$ (optimal) and 2.5 (dynamic stall) at various TI. It can be seen that:

- The sensitivity of the mean velocity in the turbine wake to TI is less than λ but more than Re_c.
- The large fluctuations in the strength of the shed vortices for TI = 0%, shown in Fig. 25, are also clearly distinguished at $x/d \leq 1.5$ where the wake is strongly influenced by the local aerodynamic of blades.
- The fluctuations in the mean velocity are more significant for $\lambda = 2.5$ due to dynamic stall on the blades and stronger fluctuations in the strength of the shed vorticity.
- As the wake travels further downstream, such fluctuations are damped out.
- The influence of TI on the mean velocity in the wake is very prominent for both optimal and dynamic stall cases. This remains non-negligible for downstream locations as far as $x/d = 4.0$.
- Increasing TI reduces the impact of the shaft on the mean velocity in the turbine wake. This is attributed to the considerable delay in separation over the shaft and the subsequent reduction of the shaft wake.
- By increasing TI, the velocity deficit in the wake and the wake expansion reduce while the wake recovery increases. The findings are in line with the role of the turbulence level on the wake of HAWTs [123].

7. Summary and conclusions

High-fidelity computational fluid dynamics (CFD) simulations, extensively validated with experiments, are performed to systematically investigate the impact of operational parameters, i.e. tip speed ratio (λ), Reynolds number (Re_c) and turbulence intensity (TI), on the power performance and aerodynamics of vertical axis wind turbines. The study investigates a wide range of the parameters: $1.2 \leq \lambda \leq 6.0$, $0.3 \times 10^5 \leq Re_c \leq 4.2 \times 10^5$ and $0\% \leq TI \leq 30\%$ to comprehensively

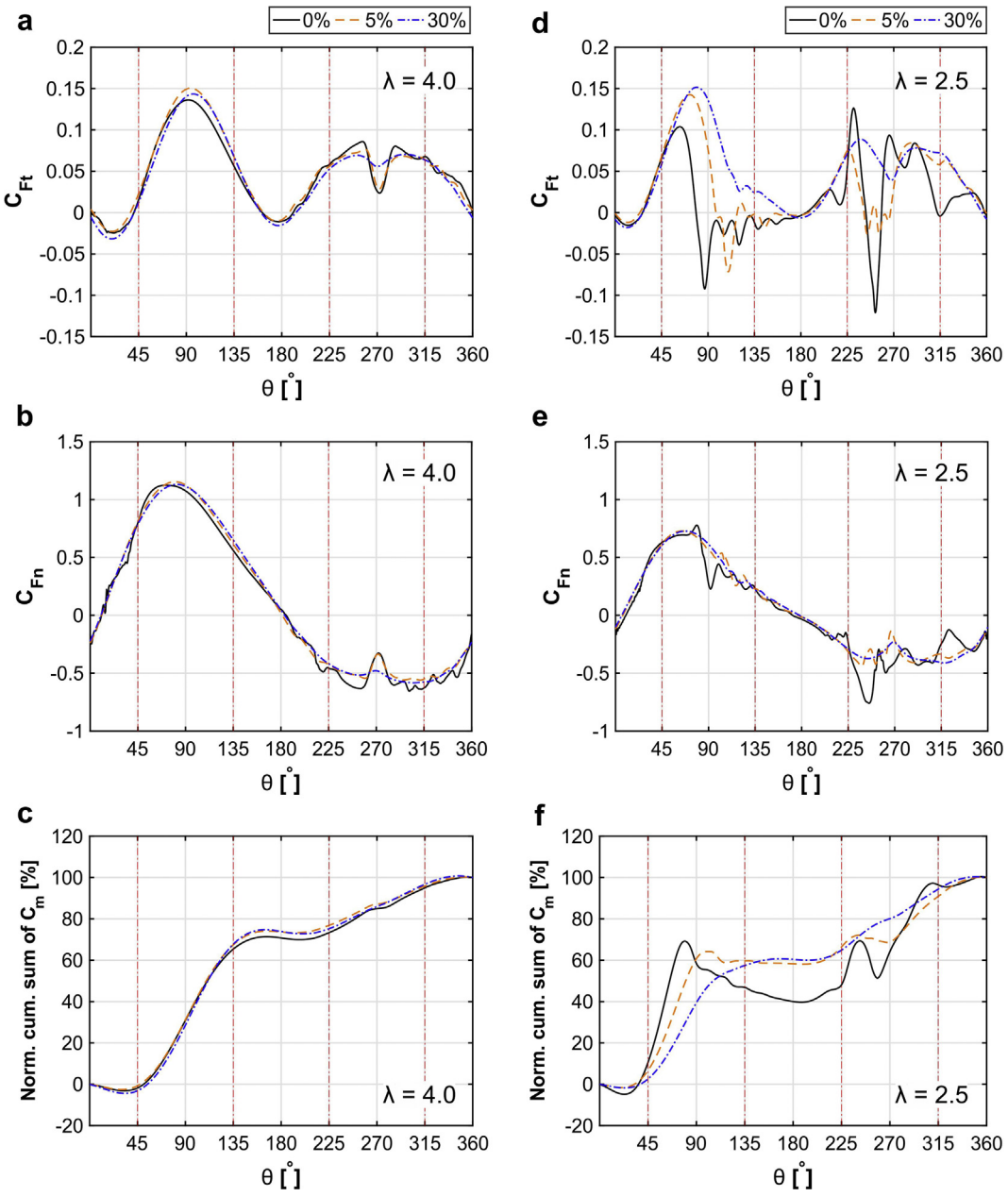

Fig. 24. Coefficients of tangential and normal force coefficients and the normalized cumulative sum of moment coefficient during the last turbine revolution for different TI at (a–c) λ = 4.0, (d–f) λ = 2.5.

clarify their impact on dynamic loads on blades, turbine performance and wake. The findings from the study can be summarized as follows:

(1) Tip speed ratio:
- In the turbine fore half, the variation of α is half-cycle sinusoidal, while in the turbine aft half it is notably different due to the strong impact of the turbine induction, the blade-wake interactions and the shaft wake. Increase of λ also increases the flatness in α curve in the turbine aft half.
- The amplitude of the oscillations in the normalized relative velocity increases from 17.5% at λ = 5.5 to 36.7% at λ = 2.5.
- For λ < 3.0, the variations of α exceed α_{ss} which leads to dynamic stall. This is accompanied by strong fluctuations in C_l and C_d and a dramatic jump in C_d. The consequent blade-wake interactions also result in strong load fluctuations in the downwind quartile. Reducing λ significantly increases $C_{l,max}$ and $C_{d,max}$.
- Reducing λ promotes laminar-to-turbulent transition, decreases the length of the laminar separation bubble and moves the trailing edge separation towards the leading edge. These occur due to the higher α of the blades.
- An optimal λ exists for C_P while C_T asymptotically increases with λ. For the studied turbine, the optimal λ is 4.0. The optimal λ stays constant with Re and reduced frequency, within the studied range.
- The contribution of different turbine quartiles to the total power production is strongly λ-dependent.
- Increasing λ increases the velocity deficit, wake expansion and streamwise asymmetry in the wake.
- The length of the turbine wake, defined at $V/U_\infty = 0.97$, decreases asymptotically by increasing λ. The decrease in the wake length is thought to be due to the amplification of instabilities due to the closer spacing of the shed vortices in the wake which could lead to an earlier break down of the wake structure.

(2) Reynolds number:
- α and normalized V_{rel} are almost Re-independent, esp. in the fore

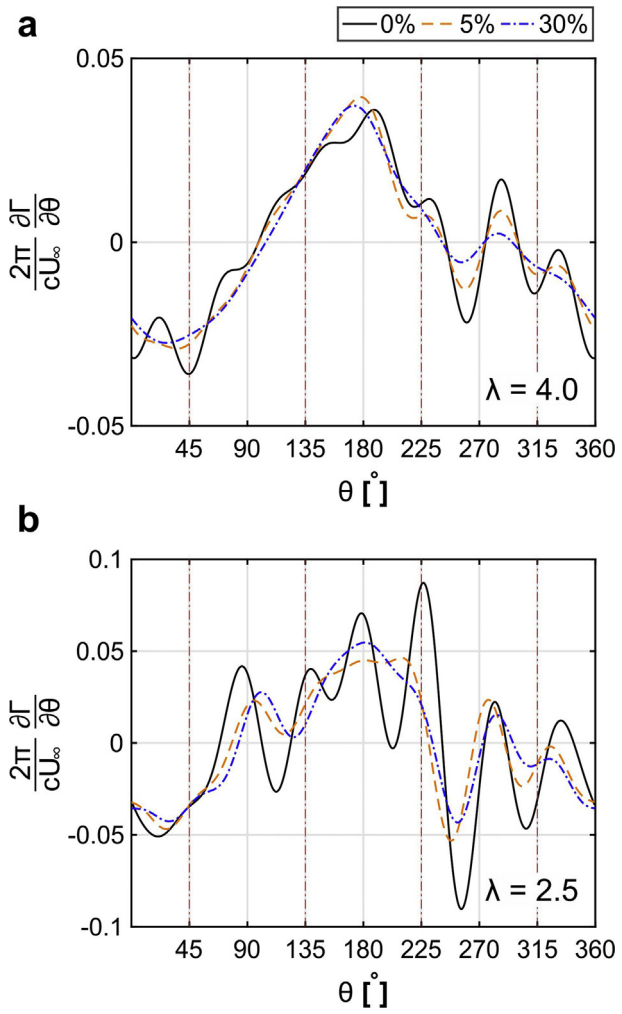

Fig. 25. Shed vorticity by a single blade during the last revolution for different TI at λ: (a) 4.0, (b) 2.5. Positive values denote counter-clockwise circulation based on the Kutta–Joukowski theorem [111].

turbine half.

- Increase of Re_c: (i) promotes the laminar-to-turbulent transition and postpones the separation on blades, (ii) reduces the fluctuations in C_l and C_d associated with the dynamic stall and the blade-wake interactions, (iii) reduces the impact of the shaft on turbine loads, (iv) improves C_l by increasing $C_{l,max}$ and delaying stall where the sensitivity of C_l to Re_c decreases for $Re_c > 10^5$, and (v) reduces C_d, especially in the turbine aft half, and $C_{d,max}$, occurring due to the blade-wake interactions.
- Within the studied range, C_P is strongly Re-dependent where the sensitivity decreases by the increase of Re_c. C_T is much less Re-dependent. For high λ, C_T is almost Re-independent.
- The optimum λ is Re-independent.
- Unlike the optimal λ of 4.0, in dynamic stall (λ = 2.5) the contribution of different quartiles to the total power production is Re-dependent.
- Within the studied range, the mean velocity in the wake is Re-dependent, while the sensitivity is lower compared to that of λ and TI. The sensitivity to Re_c does not reduce as the wake travels downstream from x/d = 1.0 to 4.0.
- Increasing Re_c increases the velocity deficit and the wake expansion.

(3) Turbulence intensity:

- α and normalized V_{rel} are almost TI-independent, except in the wake of the shaft.
- Increase of TI: (i) reduces the impact of the shaft on the turbine loads, (ii) promotes laminar-to-turbulent transition, and (iii) reduces the fluctuations in C_l and C_d associated with the dynamic stall, the blade-wake interactions and presence of the long laminar separation bubble on the blade at TI = 0%.
- At optimal λ (= 4.0), an increase of TI from 0% to 5%, reduces C_d while further increase of TI to 30% results in a significant growth in C_d due to the increased skin friction in the attached boundary layer on the blade.
- At λ = 2.5 (dynamic stall), an increase of TI to 30% reduces the $C_{d,max}$, associated with the dynamic stall and the consequent blade-wake interactions, while $C_{l,max}$ is not affected.
- C_P is strongly TI-dependent while C_T is almost TI-independent.
- The optimum λ slightly decreases by increasing TI.
- At λ = 2.5 (dynamic stall), increasing TI from 0% to 30% dramatically improves C_P by 249%. The improvement is associated to the delay in stall. For higher λ, an optimal value of TI exists. The optimal TI reduces from 15% to 5% for λ increasing from 3.0 to 5.5. At optimal λ (= 4.0), increasing TI from 0% to 5% improves C_P by 7% while further increase of TI to 30% drops C_P by 9%.
- Unlike the optimal λ of 4.0, in dynamic stall (λ = 2.5) the contribution of different quartiles to the total power production is TI-dependent.
- Mean velocity in the wake is strongly influenced by TI. The sensitivity is less than that to λ but more than that to Re.
- Increase of TI decreases the velocity deficit and the wake expansion while increases the wake recovery.

The main conclusions are:

- Two co-occurring sources of unsteadiness, α and V_{rel}, complicate the aerodynamics of VAWTs.
- Neglecting the induced velocity, via using the geometrical angle of attack, can lead to an overestimation of the variations of α up to 8.3° and the magnitude of C_d and a shift in the C_l-α and C_d-α curves, which could result in a large uncertainty in the turbine power prediction.
- Maintaining the optimal λ (at different freestream velocities) via a variable-speed VAWT substantially improves C_P compared to a fixed-speed VAWT. The improvement is 168%, for example, at 4 m/s compared to a turbine operating at a fixed rotational speed of 65.1 rad/s.
- The upwind quartile is the major contributor to the total power production with more than 50% contribution in all λ studied.
- Given the inherent unsteady nature of VAWTs, which is due to the continuous and substantial variations of angle of attack and relative velocity during each revolution, power enhancement methods such as individual blade dynamic pitching, trailing edge flaps, microtabs and other flow control methods, can hardly be made effective during the whole revolution due to practical difficulties. Therefore, because the upwind quartile plays the most important role in the turbine total power production, the use of such power enhancement methods for this quartile, rather than the whole revolution, would be less challenging and more practical in terms of energy input, system complexity and time response.
- Within the range studied, $0.3 \times 10^5 \leq Re_c \leq 4.3 \times 10^5$ and $0 \leq TI \leq 30\%$, the turbine power coefficient C_P and wake characteristics (i.e. mean velocity profile, velocity deficit and wake expansion) are strongly sensitive to Re and TI. Therefore, any experimental/numerical VAWT study performed for a scaled model (lower Re_c) or at a different turbulence level needs to consider the strong sensitivity to Re_c and TI of any measured/calculated turbine power and wake data. The influence of these parameters on the power measurements would lead to unrealistic performance prediction for the full-scale turbine while their influence on the wake measurements would play a role when the effect of the turbine wake

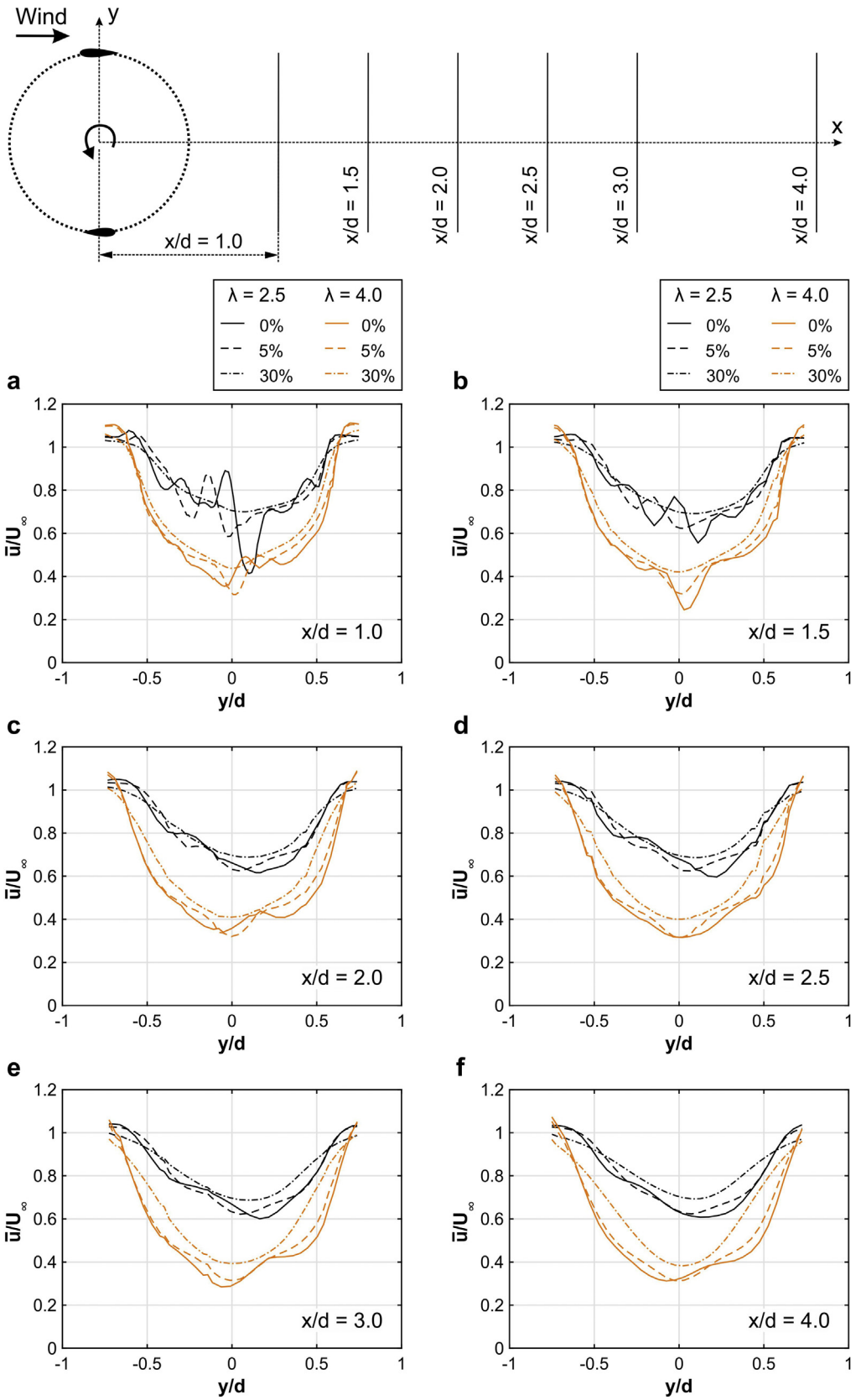

Fig. 26. Time-averaged (over the last turbine revolution) normalized (with freestream velocity) streamwise velocity along the lateral line $-0.75 \leq y/d \leq 0.75$ at several downstream locations for different TI at $\lambda = 2.5$ and 4.0.

on the downstream turbines in an array of turbines is of interest.

The findings of the current study highlight the importance of the impact of the operational parameters, i.e. λ, Re and TI, on aerodynamic performance of VAWTs. In the present study, a Darrieus H-type VAWT has been investigated. Note that the difference between the Darrieus H-type VAWT and the other types of Darrieus VAWTs, such as the Φ-type, is limited to the blade shape in spanwise direction: the former has straight blades while the latter has curved ones. Therefore, neglecting the 3D tip effects and the variations of circulation along the blade span, the 2D cross-section of the Darrieus VAWTs have similar aerodynamic behavior at a given geometrical and operational condition and will also respond similarly to the variations of the operational parameters investigated in the present study. Therefore, as the focus of the present study is on the mid-plane of the turbine, the findings on the dynamic loads on the blades will be applicable to the other types of Darrieus VAWTs as well. Considering the impact of operational parameters on the turbine performance and wake, while the observed trends could be common between the H-type configuration and the other blade configurations, there could be differences in the absolute values mainly because the H-type and also the helical blade configurations benefit from a constant radius along the blade span, which therefore means that the tip speed ratio and Re_c remains constant along the span. This is while the case is different for the other blade configurations, such Φ-type, where due to the curved blade configurations each blade section has a different radius, thus a different tip speed ratio and Re_c. Therefore, extending the current findings for these configurations needs special attention to their spanwise variations of tip speed ratio and Re_c.

Note that the evaluation is based on comprehensive analyses of a low-solidity turbine with a symmetric airfoil. Dependency of the derived conclusions on the turbine geometrical parameters are worthwhile to be investigated. In addition, the optimal value of λ, identified in this paper, is dependent on the turbine characteristics and will be different for a turbine of different solidity and/or airfoil shape. Therefore, such analysis will need to be repeated for that case to identify the optimal λ.

The range of Re investigated in this study corresponds to the regime of interest for urban VAWTs. Extension of the conclusions for higher Re, applicable to large-scale offshore VAWTs, might demand further research.

Turbulence length scale, together with TI, is another important parameter which could influence the boundary layer events, VAWT performance and wake and such investigation is recommended for future research. In addition, the use of more advanced methods, i.e. hybrid RANS-LES and LES, together with detailed wind tunnel experiments to investigate the impact of turbulence characteristics for VAWT is also proposed.

The conclusions can significantly support more accurate performance prediction of VAWTs for various operating conditions. Additionally, the results recommend that the design of VAWTs needs to steer towards optimal variable-speed operation, similar to HAWTs, while the cost effectiveness of variable-VAWTs is proposed for future research.

Acknowledgement

The authors would like to acknowledge support from the European Commission's Framework Program Horizon 2020, through the Marie Curie Innovative Training Network (ITN) AEOLUS4FUTURE - Efficient harvesting of the wind energy (H2020-MSCA-ITN-2014: Grant agreement no. 643167) and the TU1304 COST ACTION “WINERCOST”. The authors gratefully acknowledge the partnership with ANSYS CFD. This work was sponsored by NWO Exacte Wetenschappen (Physical Sciences) for the use of supercomputer facilities, with financial support from the Nederlandse Organisatie voor Wetenschappelijk Onderzoek (Netherlands Organization for Scientific Research, NWO). The 2nd author is currently a postdoctoral fellow of the Research Foundation – Flanders (FWO) and is grateful for its financial support (project FWO 12M5316N).

Appendix A. Method for calculation of the experienced angle of attack and relative velocity

For VAWTs, for simplicity it is customary to neglect the turbine induction in the performance analysis. This assumption provides the geometrical values of the relative velocity $V_{rel,geo}$ and the angle of attack α_{geo}, which are defined based on ignoring the induced velocity component of the incoming flow. Based on $V_{rel,geo}$ and α_{geo}, lift and drag coefficients are calculated which are different from the values actually experienced by the blades. The geometrical relative velocity is defined as a vector sum of the freestream velocity, $\vec{U}_\infty$, and the blade tip speed, $\vec{\Omega} \times \vec{R}$ using Eq. (1). Based on this assumption, the geometrical values of the tangential and normal velocity components (V_t and V_n) are calculated using Eqs. (2) and (3).

$$\vec{V}_{rel,geo} = (\vec{\Omega} \times \vec{R}) + \vec{U}_\infty \tag{1}$$

$$V_t = R\Omega + U_\infty \cos(\theta) \tag{2}$$

$$V_n = U_\infty \sin(\theta) \tag{3}$$

Finally, the magnitude of the geometrical relative velocity and angle of attack are calculated using Eqs. (4) and (5):

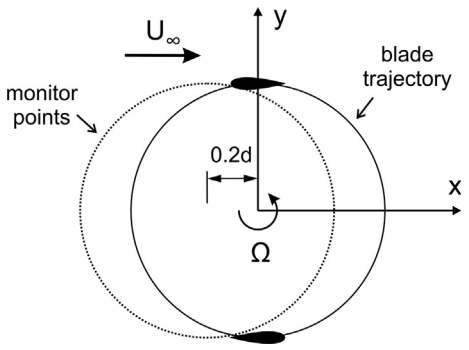

Fig. A1. Monitor points for sampling velocity components to calculate the induced velocity.

$$V_{rel,geo} = \sqrt{V_t^2 + V_n^2} = U_\infty \sqrt{\lambda^2 + 2\lambda\cos(\theta) + 1} \tag{4}$$

$$\alpha_{geo} = tan^{-1}\left(\frac{V_n}{V_t}\right) = tan^{-1}\left(\frac{\sin\theta}{\cos\theta + \lambda}\right) \tag{5}$$

The geometrical lift and drag coefficients are then calculated using Eqs. (6) and (7):

$$C_l = [C_{Ft}\sin(\alpha_{geo}) + C_{Fn}\cos(\alpha_{geo})]\frac{U_\infty^2}{V_{rel,geo}^2}\frac{d}{c} \tag{6}$$

$$C_d = [-C_{Ft}\cos(\alpha_{geo}) + C_{Fn}\sin(\alpha_{geo})]\frac{U_\infty^2}{V_{rel,geo}^2}\frac{d}{c} \tag{7}$$

On the other hand, the experienced values of the relative velocity V_{rel} and the angle of attack α are defined based on including the induced velocity U_i in the calculations using Eq. (8):

$$\vec{V_{rel}} = (\vec{\Omega} \times \vec{R}) + \vec{U_\infty} + \vec{U_i} \tag{8}$$

In practice, obtaining the value of U_i is challenging as the flow in the vicinity of the blade is highly influenced by the local bound circulation around the blade. Following the method proposed in Ref. [23], U_i is calculated using the flow velocity components sampled at monitoring points on a circular path with a fixed distance, i.e. 0.2d, upstream of the turbine. In the present study, the distance is found as the minimum distance where the impact of local bound circulation around the blade is minimally affecting the incoming flow. Note that based on the turbines characteristics, the monitoring circle could be selected closer to the turbine or might need to be shifted further upstream, to minimize the local blade effects, where the minimum distance can be figured out by testing a few arbitrary distances in the vicinity of the minimum value obtained in the current study, e.g. 0.1d and 0.3d. A schematic illustrating the employed monitor points is shown in Fig. A1.

The sampled instantaneous velocity components (u,v) are then averaged over one turbine revolution (3600 time-steps) both to filter out the local effects of blades passing and to represent the turbine time-averaged incoming flow over one turbine revolution. The time-averaged velocity components ($\overline{u}$, $\overline{v}$) are then employed to calculate the U_i using Eq. (9):

$$\overrightarrow{\overline{U_i}} = (\overline{u} - U_\infty, \overline{v}) \tag{9}$$

The experienced values of the tangential and the normal velocities, the relative velocity and the angle of attack can be calculated using Eqs. (10)–(13):

$$V_t = R\Omega + \overline{u}\cos(\theta) + \overline{v}\sin(\theta) \tag{10}$$

$$V_n = \overline{u}\sin(\theta) + \overline{v}\cos(\theta) \tag{11}$$

$$V_{rel} = \sqrt{V_t^2 + V_n^2} \tag{12}$$

$$\alpha = tan^{-1}\left(\frac{V_n}{V_t}\right) \tag{13}$$

The experienced lift and drag coefficients are then calculated using Eqs. (14) and (15):

$$C_l = [C_{Ft}\sin(\alpha) + C_{Fn}\cos(\alpha)]\frac{U_\infty^2}{V_{rel}^2}\frac{d}{c} \tag{14}$$

$$C_d = [-C_{Ft}\cos(\alpha) + C_{Fn}\sin(\alpha)]\frac{U_\infty^2}{V_{rel}^2}\frac{d}{c} \tag{15}$$

Fig. A2 presents the experienced and geometrical values of angle of attack, relative velocity, lift and drag coefficients for three different tip speed ratios. By comparing the geometrical and experienced values, several noticeable differences are observed:

- The overall variations of α are significantly different from a fully sinusoidal function which is the case for α_{geo}.
- At $\theta = 0^\circ$ and 180°, due to the lateral deviation of the flow at the turbine incidence (streamtube expansion), α has a negative non-zero value. This is while α_{geo} always predicts zero value at such θ.
- The impact of the shaft wake on α, which is seen as a sudden reduction in magnitude, is neglected by α_{geo}.
- For all cases, α_{geo} overestimates the amplitude of variations compared to α. This is due to ignoring the induced velocity by the turbine. In the turbine fore half, the overestimation is approximately 2.0°, while this value goes up to 8.3° in the turbine aft half. In the turbine fore half, the trend of α_{geo} is similar to that of α. However, significant differences are present in the turbine aft half.
- The geometrical and experienced values of relative velocity are also noticeably different, esp. in the turbine aft half.
- During the fore turbine half, the experienced C_l is slightly higher that the geometrical values at the same azimuthal position while the experienced C_l - α curve is considerably shifted upward compared to the geometrical one.
- The experienced C_d is significantly lower than the geometrical one almost during the whole revolution.
- The slope of C_d curve is lower for the experienced values (Fig. A2f), while no significant difference in slope is observed for C_l (Fig. A2e).
- $C_{d,max}$ is significantly overestimated by geometrical values while $C_{l,max}$ is slightly underestimated. Both values occur at higher α compared to the experienced values.
- The magnitude of asymmetry (hysteresis) in dynamic load variations (the absolute difference between the higher and lower values of C_l and C_d at selfsame α) is almost the same for geometrical and experienced polars.

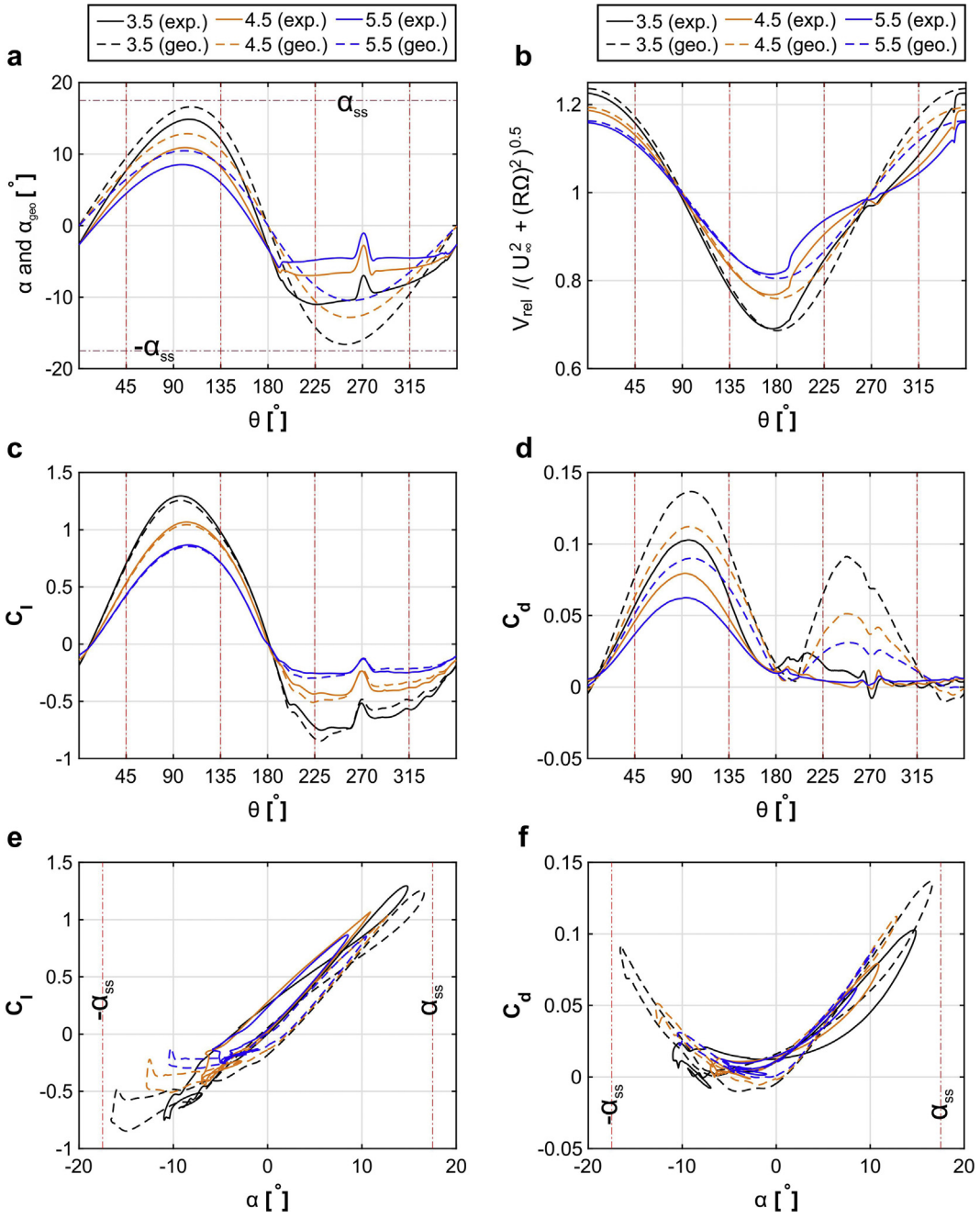

Fig. A2. Experienced (exp.) and geometrical (geo.) values of angle of attack, relative velocity, lift and drag coefficients during the last turbine revolution for different tip speed ratios. α_{ss} denotes the inviscid static stall angle from Xfoil [106]. ($Re_c \approx 2.0 \times 10^5$).

Therefore, although α_{geo} can be employed to provide a first approximation of $\Delta\alpha$ with respect to the tip speed ratio for VAWTs, special attention should be paid to the non-negligible differences between the geometrical and experienced angle of attack, relative velocity, lift and drag coefficients.

References

[1] Wang Y, Sun X, Dong X, Zhu B, Huang D, Zheng Z. Numerical investigation on aerodynamic performance of a novel vertical axis wind turbine with adaptive blades. Energy Convers Manage 2016;108:275–86.

[2] Tahani M, Babayan N, Mehrnia S, Shadmehri M. A novel heuristic method for optimization of straight blade vertical axis wind turbine. Energy Convers Manage 2016;127:461–76.

[3] Shahizare B, Nik-Ghazali N, Chong WT, Tabatabaeikia S, Izadyar N, Esmaeilzadeh A. Novel investigation of the different omni-direction-guide-vane angles effects on the urban vertical axis wind turbine output power via three-dimensional numerical simulation. Energy Convers Manage 2016;117:206–17.

[4] Scungio M, Arpino F, Focanti V, Profili M, Rotondi M. Wind tunnel testing of scaled models of a newly developed Darrieus-style vertical axis wind turbine with auxiliary straight blades. Energy Convers Manage 2016;130:60–70.

[5] Bianchini A, Balduzzi F, Ferrara G, Ferrari L. Virtual incidence effect on rotating airfoils in Darrieus wind turbines. Energy Convers Manage 2016;111:329–38.

[6] Bianchini A, Balduzzi F, Bachant P, Ferrara G, Ferrari L. Effectiveness of two-dimensional CFD simulations for Darrieus VAWTs: a combined numerical and experimental assessment. Energy Convers Manage 2017;136:318–28.

[7] Zanforlin S. Advantages of vertical axis tidal turbines set in close proximity: A comparative CFD investigation in the English Channel. Ocean Eng 2018;156:358–72.

[8] Borg M, Shires A, Collu M. Offshore floating vertical axis wind turbines, dynamics modelling state of the art. Part I: aerodynamics. Renew Sustain Energy Rev 2014;39:1214–25.
[9] Paulsen US, Madsen HA, Kragh KA, Nielsen PH, Baran I, Hattel J, et al. DeepWind-from idea to 5 MW concept. Energy Procedia 2014;53:23–33.
[10] Bedon G, Schmidt Paulsen U, Aagaard Madsen H, Belloni F, Raciti Castelli M, Benini E. Computational assessment of the DeepWind aerodynamic performance with different blade and airfoil configurations. Appl Energy 2017;185(2):1100–8.
[11] van Hooff T, Blocken B, Aanen L, Bronsema B. A venturi-shaped roof for wind-induced natural ventilation of buildings: wind tunnel and CFD evaluation of different design configurations. Build Environ 2011;46(9):1797–807.
[12] Tummala A, Velamati RK, Sinha DK, Indraja V, Krishna VH. A review on small scale wind turbines. Renew Sustain Energy Rev 2016;56:1351–71.
[13] Toja-Silva F, Colmenar-Santos A, Castro-Gil M. Urban wind energy exploitation systems: behaviour under multidirectional flow conditions—opportunities and challenges. Renew Sustain Energy Rev 2013;24:364–78.
[14] Aslam Bhutta MM, Hayat N, Farooq AU, Ali Z, Jamil SR, Hussain Z. Vertical axis wind turbine – a review of various configurations and design techniques. Renew Sustain Energy Rev 2012;16(4):1926–39.
[15] Yang A-S, Su Y-M, Wen C-Y, Juan Y-H, Wang W-S, Cheng C-H. Estimation of wind power generation in dense urban area. Appl Energy 2016;171:213–30.
[16] Blocken B, Moonen P, Stathopoulos T, Carmeliet J. Numerical study on the existence of the Venturi effect in passages between perpendicular buildings. J Eng Mech 2008;134(12):1021–8.
[17] Park JH, Chung MH, Park JC. Development of a small wind power system with an integrated exhaust air duct in high-rise residential buildings. Energy Build 2016;122:202–10.
[18] Antoniou N, Montazeri H, Wigo H, Neophytou MKA, Blocken B, Sandberg M. CFD and wind-tunnel analysis of outdoor ventilation in a real compact heterogeneous urban area: evaluation using "air delay". Build Environ 2017;126:355–72.
[19] Rezaeian M, Montazeri H, and Loonen R, "Science foresight using life-cycle analysis, text mining and clustering: a case study on natural ventilation," Technological Forecasting & Social Change, vol. 118 (C), pp. 270–280, 2017.
[20] Montazeri H, Montazeri F. CFD simulation of cross-ventilation in buildings using rooftop wind-catchers: impact of outlet openings. Renewable Energy 2018;118:502–20.
[21] Montazeri H, Montazeri F, Azizian R, Mostafavi S. Two-sided wind catcher performance evaluation using experimental, numerical and analytical modeling. Renewable Energy 2010;35(7):1424–35.
[22] Montazeri H. Experimental and numerical study on natural ventilation performance of various multi-opening wind catchers. Build Environ 2011;46(2):370–8.
[23] Rezaeiha A, Kalkman I, Blocken B. Effect of pitch angle on power performance and aerodynamics of a vertical axis wind turbine. Appl Energy 2017;197:132–50.
[24] Simão Ferreira C, Scheurich F. Demonstrating that power and instantaneous loads are decoupled in a vertical-axis wind turbine. Wind Energy 2014;17(3):385–96.
[25] Chen W-H, Chen C-Y, Huang C-Y, Hwang C-J. Power output analysis and optimization of two straight-bladed vertical-axis wind turbines. Appl Energy 2017;185:223–32.
[26] Borg M, Collu M. Frequency-domain characteristics of aerodynamic loads of offshore floating vertical axis wind turbines. Appl Energy 2015;155:629–36.
[27] Carbó Molina A, Bartoli G, and De Troyer T, "Generation of uniform turbulence profiles in the wind tunnel for urban VAWT testing," in Wind Energy Exploitation in Urban Environment: TUrbWind 2017 Colloquium, ed: Springer International Publishing, 2018, pp. 27–43.
[28] Carbó Molina A, Bartoli G, de Troyer T. Wind tunnel testing of small vertical-axis wind turbines in turbulent flows. Procedia Eng 2017;199:3176–81.
[29] Eriksson S, Bernhoff H, Leijon M. Evaluation of different turbine concepts for wind power. Renew Sustain Energy Rev 2008;12(5):1419–34.
[30] Chong W-T, Muzammil WK, Wong K-H, Wang C-T, Gwani M, Chu Y-J, et al. Cross axis wind turbine: pushing the limit of wind turbine technology with complementary design. Appl Energy 2017;207:78–95.
[31] Govind B. Increasing the operational capability of a horizontal axis wind turbine by its integration with a vertical axis wind turbine. Appl Energy 2017;199:479–94.
[32] Rezaeiha A, Pereira R, and Kotsonis M, "Fluctuations of angle of attack and lift coefficient and the resultant fatigue loads for a large horizontal axis wind turbine," Renewable Energy, vol. 114 (B), pp. 904–916, 2017.
[33] Joselin Herbert GM, Iniyan S, Sreevalsan E, Rajapandian S. A review of wind energy technologies. Renew Sustain Energy Rev 2007;11(6):1117–45.
[34] Araya DB, Dabiri JO. Vertical axis wind turbine in a falling soap film. Phys Fluids 2015;27(9):091108.
[35] Kinzel M, Araya DB, Dabiri JO. Turbulence in vertical axis wind turbine canopies. Phys Fluids 2015;27(11):115102.
[36] Brownstein ID, Kinzel M, Dabiri JO. Performance enhancement of downstream vertical-axis wind turbines. J Renewable Sustainable Energy 2016;8(5):053306.
[37] Ryan KJ, Coletti F, Elkins CJ, Dabiri JO, and Eaton JK, "Three-dimensional flow field around and downstream of a subscale model rotating vertical axis wind turbine," Experiments in Fluids, vol. 57 (3), 2016.
[38] Abkar M, Dabiri JO. Self-similarity and flow characteristics of vertical-axis wind turbine wakes: an LES study. J Turbul 2017;18(4):373–89.
[39] Araya DB, Colonius T, Dabiri JO. Transition to bluff-body dynamics in the wake of vertical-axis wind turbines. J Fluid Mech 2017;813:346–81.
[40] Pope K, Dincer I, Naterer GF. Energy and exergy efficiency comparison of horizontal and vertical axis wind turbines. Renewable Energy 2010;35(9):2102–13.
[41] Simão Ferreira C, van Zuijlen A, Bijl H, van Bussel G, van Kuik G. Simulating dynamic stall in a two-dimensional vertical-axis wind turbine: verification and validation with particle image velocimetry data. Wind Energy 2010;13(1):1–17.
[42] Simão Ferreira C, van Kuik G, van Bussel G, Scarano F. Visualization by PIV of dynamic stall on a vertical axis wind turbine. Exp Fluids 2008;46(1):97–108.
[43] Amet E, Maître T, Pellone C, and Achard JL, "2D numerical simulations of blade-vortex interaction in a Darrieus turbine," Journal of Fluids Engineering, vol. 131 (11), pp. 111103(1–15), 2009.
[44] Bianchini A, Balduzzi F, Rainbird JM, Peiro J, Graham JMR, Ferrara G, and Ferrari L, "An experimental and numerical assessment of airfoil polars for use in Darrieus wind turbines—part I: flow curvature effects," Journal of Engineering for Gas Turbines and Power, vol. 138 (032602), 2015.
[45] Tsai H-C, Colonius T. Coriolis effect on dynamic stall in a vertical axis wind turbine. AIAA Journal 2016;54(1):216–26.
[46] Delafin PL, Nishino T, Wang L, Kolios A. Effect of the number of blades and solidity on the performance of a vertical axis wind turbine. J Phys Conf Ser 2016;753:022033.
[47] Cheng Z, Madsen HA, Gao Z, Moan T. Effect of the number of blades on the dynamics of floating straight-bladed vertical axis wind turbines. Renewable Energy 2017;101:1285–98.
[48] Li Qa, Maeda T, Kamada Y, Murata J, Furukawa K, and Yamamoto M, "Effect of number of blades on aerodynamic forces on a straight-bladed Vertical Axis Wind Turbine," *Energy,* vol. 90, pp. 784-795, 2015.
[49] Li Q, Maeda T, Kamada Y, Shimizu K, Ogasawara T, Nakai A, et al. Effect of rotor aspect ratio and solidity on a straight-bladed vertical axis wind turbine in three-dimensional analysis by the panel method. Energy 2017;121:1–9.
[50] Li Q, Maeda T, Kamada Y, Murata J, Shimizu K, Ogasawara T, et al. Effect of solidity on aerodynamic forces around straight-bladed vertical axis wind turbine by wind tunnel experiments (depending on number of blades). Renewable Energy 2016;96:928–39.
[51] Eboibi O, Danao LAM, Howell RJ. Experimental investigation of the influence of solidity on the performance and flow field aerodynamics of vertical axis wind turbines at low Reynolds numbers. Renewable Energy 2016;92:474–83.
[52] Simão Ferreira C, Geurts B. Aerofoil optimization for vertical-axis wind turbines. Wind Energy 2014;18(8):1371–85.
[53] Bedon G, De Betta S, Benini E. Performance-optimized airfoil for Darrieus wind turbines. Renewable Energy 2016;94:328–40.
[54] Sengupta AR, Biswas A, Gupta R. Studies of some high solidity symmetrical and unsymmetrical blade H-Darrieus rotors with respect to starting characteristics, dynamic performances and flow physics in low wind streams. Renewable Energy 2016;93:536–47.
[55] Rezaeiha A, Kalkman I, Montazeri H, and Blocken B, "Effect of the shaft on the aerodynamic performance of urban vertical axis wind turbines," Energy Conversion and Management, vol. 149 (C), pp. 616–630, 2017.
[56] Alaimo A, Esposito A, Messineo A, Orlando C, Tumino D. 3D CFD analysis of a vertical axis wind turbine. Energies 2015;8(4):3013–33.
[57] Parker CM and Leftwich MC, "The effect of tip speed ratio on a vertical axis wind turbine at high Reynolds numbers," Experiments in Fluids, vol. 57 (5), 2016.
[58] Möllerström E, Ottermo F, Goude A, Eriksson S, Hylander J, Bernhoff H. Turbulence influence on wind energy extraction for a medium size vertical axis wind turbine. Wind Energy 2016;19:1963–73.
[59] Armstrong S, Fiedler A, Tullis S. Flow separation on a high Reynolds number, high solidity vertical axis wind turbine with straight and canted blades and canted blades with fences. Renewable Energy 2012;41:13–22.
[60] Paraschivoiu I, Desy P. Aerodynamics of small-scale vertical-axis wind turbines. J Propul Power 1986;2(3):282–8.
[61] Araya DB and Dabiri JO, "A comparison of wake measurements in motor-driven and flow-driven turbine experiments," Experiments in Fluids, vol. 56 (7), 2015.
[62] Blackwell B, Sheldahl R, Feltz L. "Wind tunnel performance data for the Darrieus wind turbine with NACA0012 blades; SAND76-0130," Sandia National Laboratories: Albuquerque. USA: NM; 1976.
[63] Polagye BL, Cavagnaro RJ, and Niblick AL, "Micropower from tidal turbines," in Proceedings of the ASME Fluids Engineering Division Summer Meeting, Incline Village, NV, USA, 2013.
[64] Bravo R, Tullis S, and Ziada S, "Performance testing of a small vertical-axis wind turbine," in Proceedings of the 21st Canadian Congress of Applied Mechanics CANCAM, Toronto, ON, Canada, 2007.
[65] Bachant P and Wosnik M, "Effects of Reynolds number on the energy conversion and near-wake dynamics of a high solidity vertical-axis cross-flow turbine," Energies, vol. 9 (73), 2016.
[66] Siddiqui MS, Rasheed A, Kvamsdal T, Tabib M. Effect of turbulence intensity on the performance of an offshore vertical axis wind turbine. Energy Procedia 2015;80:312–20.
[67] Möllerström E, Eriksson S, Goude A, Ottermo F, and Hylander J. Turbulence influence on optimum tip speed ratio for a 200 kW vertical axis wind turbine. Journal of Physics: Conference Series, vol. 753 (032048), 2016.
[68] Ahmadi-Baloutaki M, Ting DS-K, Carriveau R. The role of free-stream turbulence on flow evolution in the wake of a VAWT blade. Wind Eng 2013;37(4):401–20.
[69] Kim D-H, Chang J-W. Low-Reynolds-number effect on the aerodynamic characteristics of a pitching NACA0012 airfoil. Aerosp Sci Technol 2014;32(1):162–8.
[70] Wang S, Zhou Y, Alam MM, Yang H. Turbulent intensity and Reynolds number effects on an airfoil at low Reynolds numbers. Phys Fluids 2014;26(11):115107.
[71] Kim D-H, Chang J-W, Chung J. Low-Reynolds-number effect on aerodynamic characteristics of a NACA 0012 airfoil. J Aircraft 2011;48(4):1212–5.
[72] Gad-el-Hak M, Bandyopadhyay PR. Reynolds number effects in wall-bounded turbulent flows. Appl Mech Rev 1994;47(8):307–65.
[73] Carmichael BH. Low Reynolds number airfoil survey: vol. 1. NASA-CR-165803, USA, 1981.
[74] Lissaman PBS. Low-Reynolds-number airfoils. Annu Rev Fluid Mech

1983;15:223–39.
[75] Jacobs EN, Sherman A. Airfoil section characteristics as affected by variation of the Reynolds number, Report No. 586. Langley Field, VA, USA: National Advisory Committee for Aeronautics; 1937.
[76] Zanforlin S, Deluca S. Effects of the Reynolds number and the tip losses on the optimal aspect ratio of straight-bladed Vertical Axis Wind Turbines. Energy 2018;148:179–95.
[77] Fransson JHM, Matsubara M, Alfredsson PH. Transition induced by free-stream turbulence. J Fluid Mech 2005;527:1–25.
[78] Kosasih B, Saleh Hudin H. Influence of inflow turbulence intensity on the performance of bare and diffuser-augmented micro wind turbine model. Renewable Energy 2016;87:154–67.
[79] Sunderland K, Woolmington T, Blackledge J, Conlon M. Small wind turbines in turbulent (urban) environments: a consideration of normal and Weibull distributions for power prediction. J Wind Eng Ind Aerodyn 2013;121:70–81.
[80] Brandt L, Schlatter P, Henningson DS. Transition in boundary layers subject to free-stream turbulence. J Fluid Mech 2004;517:167–98.
[81] Goldstein ME, "Effect of free-stream turbulence on boundary layer transition," Philos Trans A Math Phys Eng Sci, vol. 372 (2020), Jul 28 2014.
[82] Tescione G, Ragni D, He C, Simão Ferreira C, van Bussel GJW. Near wake flow analysis of a vertical axis wind turbine by stereoscopic particle image velocimetry. Renewable Energy 2014;70:47–61.
[83] Blocken B, Carmeliet J, Stathopoulos T. CFD evaluation of wind speed conditions in passages between parallel buildings—effect of wall-function roughness modifications for the atmospheric boundary layer flow. J Wind Eng Ind Aerodyn 2007;95(9–11):941–62.
[84] Blocken B, Stathopoulos T, Carmeliet J. CFD simulation of the atmospheric boundary layer: wall function problems. Atmos Environ 2007;41(2):238–52.
[85] Blocken B. 50 years of computational wind engineering: past, present and future. J Wind Eng Ind Aerodyn 2014;129:69–102.
[86] Blocken B. Computational Fluid Dynamics for urban physics: Importance, scales, possibilities, limitations and ten tips and tricks towards accurate and reliable simulations. Build Environ 2015;91:219–45.
[87] Rezaeiha A, Kalkman I, Blocken B. CFD simulation of a vertical axis wind turbine operating at a moderate tip speed ratio: guidelines for minimum domain size and azimuthal increment. Renewable Energy 2017;107:373–85.
[88] Andersen SJ, Sorensen JN, and Mikkelsen RF. Turbulence and entrainment length scales in large wind farms. Philos Trans A Math Phys Eng Sci, vol. 375 (2091), Apr 13 2017.
[89] Hand B, Cashman A. Conceptual design of a large-scale floating offshore vertical axis wind turbine. Energy Procedia 2017;142:83–8.
[90] Rezaeiha A, Montazeri H, and Blocken B. Towards accurate CFD simulations of vertical axis wind turbines at different tip speed ratios and solidities: guidelines for azimuthal increment, domain size and convergence. Energy Conversion and Management, vol. 156 (C), pp. 301–316, 2018.
[91] Zhang W, Cheng W, Gao W, Qamar A, Samtaney R. Geometrical effects on the airfoil flow separation and transition. Comput Fluids 2015;116:60–73.
[92] You D, Ham F, Moin P. Discrete conservation principles in large-eddy simulation with application to separation control over an airfoil. Phys Fluids 2008;20(10):101515.
[93] Simão Ferreira C. The near wake of the VAWT: 2D and 3D views of the VAWT aerodynamics. TU Delft: PhD; 2009.
[94] Menter FR, Langtry RB, Likki SR, Suzen YB, Huang PG, Völker S. A correlation-based transition model using local variables—part I: model formulation. J Turbomach 2006;128(3):413–22.
[95] Menter FR, Kuntz M, and Langtry R. Ten years of industrial experience with the SST turbulence model. in Turbulence, Heat and Mass Transfer. vol. 4, ed, 2003.
[96] Menter FR. Two-equation eddy-viscosity turbulence models for engineering applications. AIAA Journal 1994;32(8):1598–605.
[97] Suzen YB and Huang PG. Modeling of flow transition using an intermittency transport equation. NASA/CR-1999-209313, 1999.
[98] Langtry RB, Menter FR, Likki SR, Suzen YB, Huang PG, Völker S. A correlation-based transition model using local variables—part II: test cases and industrial applications. J Turbomach 2006;128(3):423–34.
[99] Suzen YB, Huang PG, Hultgren LS, Ashpis DE. Predictions of separated and transitional boundary layers under low-pressure turbine airfoil conditions using an intermittency transport equation. J Turbomach 2003;125(3):455.
[100] Menter FR, Langtry R, Völker S. Transition modelling for general purpose CFD codes. Flow, Turbulence Combustion 2006;77(1–4):277–303.
[101] Rezaeiha A, Montazeri H, and Blocken B. CFD simulations of vertical axis wind turbines: guidelines for the choice of turbulence model. In preparation, 2018.
[102] Roache PJ. Quantification of uncertainty in computational fluid dynamics. Annu Rev Fluid Mech 1997;29:123–60.
[103] Gad-el-Hak M, Bushnell DM. Separation control: review. J Fluids Eng 1991;113(1):5–30.
[104] Castelli MR, Englaro A, Benini E. The Darrieus wind turbine: proposal for a new performance prediction model based on CFD. Energy 2011;36(8):4919–34.
[105] Rezaeiha A, Montazeri H, and Blocken B. Impact of geometrical parameters on aerodynamic performance of vertical axis wind turbines. Submitted, 2018.
[106] Drela M, "XFOIL: an analysis and design system for low Reynolds number airfoils," in Low Reynolds Number Aerodynamics: Vol. 54 of the series 'Lecture Notes in Engineering', ed: Springer, 1989, pp. 1–12.
[107] Lee T, Gerontakos P. Investigation of flow over an oscillating airfoil. J Fluid Mech 2004;512:313–41.
[108] O'Meara M, Mueller TJ. Laminar separation bubble characteristics on an airfoil at low Reynolds numbers. AIAA J 1987;25(8):1033–41.
[109] Nati A, de Kat R, Scarano F, and van Oudheusden BW. Dynamic pitching effect on a laminar separation bubble. Experiments in Fluids, vol. 56 (9), 2015.
[110] Bachant P, Wosnik M. Characterising the near-wake of a cross-flow turbine. J Turbul 2015;16(4):392–410.
[111] Anderson JD. Fundamental of aerodynamics. Boston: McGraw-Hill; 2001.
[112] Vermeer L, Sørensen JN, Crespo A. Wind turbine wake aerodynamics. Prog Aerosp Sci 2003;39:467–510.
[113] Pitteloud JD and Gsänger S. Small wind world report summary. World Wind Energy Association (WWEA), 2017.
[114] Islam MR, Mekhilef S, Saidur R. Progress and recent trends of wind energy technology. Renew Sustain Energy Rev 2013;21:456–68.
[115] Singleton JD, Yeager Jr. WT. Important scaling parameters for testing model-scale helicopter rotors. J Aircraft 2000;37:396–402.
[116] Bousman WG, "Evaluation of airfoil dynamic stall characteristics for maneuverability," in Proceedings of the 26th European Rotorcraft Forum, The Hague, The Netherlands, 26–29 Sep. 2000.
[117] Kotsonis M, Pul R, and Veldhuis L. Influence of circulation on a rounded-trailing-edge airfoil using plasma actuators. Experiments in Fluids, vol. 55 (7), 2014.
[118] Yoon HS, Hill DF, Balachandar S, Adrian RJ, Ha MY. Reynolds number scaling of flow in a Rushton turbine stirred tank. Part I—Mean flow, circular jet and tip vortex scaling. Chem Eng Sci 2005;60(12):3169–83.
[119] Chamorro LP, Arndt REA, Sotiropoulos F. Reynolds number dependence of turbulence statistics in the wake of wind turbines. Wind Energy 2012;15(5):733–42.
[120] McTavish S, Feszty D, Nitzsche F. Evaluating Reynolds number effects in small-scale wind turbine experiments. J Wind Eng Ind Aerodyn 2013;120:81–90.
[121] Bearman PW, Morel T. Effect of free stream turbulence on the flow around bluff bodies. Prog Aerosp Sci 1983;20:97–123.
[122] Simoni D, Lengani D, Ubaldi M, Zunino P, and Dellacasagrande M,. Inspection of the dynamic properties of laminar separation bubbles: free-stream turbulence intensity effects for different Reynolds numbers. Experiments in Fluids, vol. 58 (6), 2017.
[123] Jin Y, Liu H, Aggarwal R, Singh A, Chamorro L. Effects of freestream turbulence in a model wind turbine wake. Energies 2016;9(10):830.